Accepted Manuscript

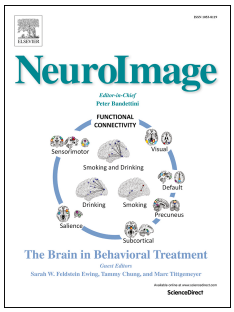

Simultaneous resting-state FDG-PET/fMRI in Alzheimer Disease: Relationship between glucose metabolism and intrinsic activity

Rocco Marchitelli, Marco Aiello, Arnaud Cachia, Mario Quarantelli, Carlo Cavaliere, Alfredo Postiglione, Gioacchino Tedeschi, Patrizia Montella, Graziella Milan, Marco Salvatore, Elena Salvatore, Jean Claude Baron, Sabina Pappatà

PII: S1053-8119(18)30358-6

DOI: 10.1016/j.neuroimage.2018.04.048

Reference: YNIMG 14895

To appear in: *NeuroImage*

Received Date: 27 October 2017

Revised Date: 18 April 2018

Accepted Date: 20 April 2018

Please cite this article as: Marchitelli, R., Aiello, M., Cachia, A., Quarantelli, M., Cavaliere, C., Postiglione, A., Tedeschi, G., Montella, P., Milan, G., Salvatore, M., Salvatore, E., Baron, J.C., Pappatà, S., Simultaneous resting-state FDG-PET/fMRI in Alzheimer Disease: Relationship between glucose metabolism and intrinsic activity, *NeuroImage* (2018), doi: 10.1016/j.neuroimage.2018.04.048.

Simultaneous Resting-State FDG-PET/fMRI in Alzheimer Disease: Relationship Between Glucose Metabolism and Intrinsic Activity

Rocco Marchitelli[1†], Marco Aiello[1†*], Arnaud Cachia[2], Mario Quarantelli[3], Carlo Cavaliere[1], Alfredo Postiglione[4], Gioacchino Tedeschi[5], Patrizia Montella[5], Graziella Milan[6], Marco Salvatore[1], Elena Salvatore[7], Jean Claude Baron[8**], Sabina Pappatà[3**].

[1] IRCCS SDN, Institute of Nuclear and Diagnostic Research, Via E. Gianturco, 113, 80143 Naples, Italy.

[2] INSERM U894, Université Paris Descartes, Centre Hospitalier Sainte-Anne, Sorbonne Paris Cité, Paris, France; CNRS U8240, Université Paris Descartes, Sorbonne Paris Cité, Paris, France; Institut Universitaire de France, Paris, France.

[3] Institute of Biostructure and Bioimaging, National Research Council, Naples, Italy.

[4] Department of Clinical Medicine & Surgery, University of Naples "Federico II", Naples, Italy.

[5] Dept of Medical, Surgical, Neurological, Metabolic and Aging Sciences. University of Campania "L. Vanvitelli".

[6] Centro Geriatrico Frullone, ASL Napoli 1 Centro, Naples, Italy.

[7] Department of Neuroscience Reproductive Sciences and Odontostomatology, Federico II University, Naples, Italy.

[8] Dept of Neurology, Centre Hospitalier Sainte-Anne, Université Paris Descartes, INSERM U894, Paris, France.

† These authors equally contributed to this work.

** These authors share senior authorship.

* Corresponding author:

Marco Aiello, Ph.D.,

IRCCS SDN,

Via Gianturco 113, 80143, Naples, Italy

maiello@sdn-napoli.it

Glossary

AchEI: Anti-cholinesterase; ACC: Anterior Cingulate Cortex; AD: Alzheimer's Disease; AFNI: Analysis of Functional NeuroImages; MCI: Mild Cognitive Impairment; Aβ: Amyloid β; BET: Brain Extraction Tool; BOLD: Blood-Oxygen Level-Dependent; CDR: Clinical Dementia Rating; CI: Confidence Interval; COM: Centre Of Mass; CSF: Cerebral Spinal Fluid; DICOM: Digital Imaging and Communications in Medicine; DMN: Default Mode Network; DWI: Diffusion Weighted Imaging; EANM: European Association of Nuclear Medicine; EPI: Echo-Planar Imaging; fALFF: Fractional Amplitude of Low Frequency Fluctuations; FD: Framewise Displacements; FDG-PET: Fludeoxyglucose Positron Emission Tomography; FLAIR: FLuid-Attenuated Inversion Recovery; FWHM: Full-Width at Half-Maximum; gICA-DR: group Independent Component Analysis and Dual Regression; GLUT3: Glucose Transporter 3; GM/WM: Grey/White Matter; IPL: Inferior Parietal Lobule; IRCCS: Istituto di Ricovero e Cura a Carattere Scientifico; MELODIC: Multivariate Exploratory Linear Optimized Decomposition into Independent Components; MMSE: Mini Mental Status Examination; MPRAGE: Magnetization-Prepared Rapid Acquisition Gradient-Echo; MRI: Magnetic Resonance Imaging; MTG: Middle Temporal gyrus; NIfTI: Neuroimaging Informatics Technology Initiative; OSEM: Ordered Subset-Expectation Maximization; Pressure of Carbon DiOxide (pCO2); PCC: Posterior Cingulate Cortex; ReHo: Regional Homogeneity; ROI: Region of Interest; rs-fMRI: Resting-State Functional MRI; SFG: Superior Frontal gyrus; STG: Superior Temporal gyri; SUVR: standardized uptake value ratio; TSE: Turbo Spin Echo.

Abstract

Simultaneously evaluating resting-state brain glucose metabolism and intrinsic functional activity has potential to impact the clinical neurosciences of Alzheimer Disease (AD). Indeed, integrating such combined information obtained in the same physiological setting may clarify how impairments in neuroenergetic and neuronal function interact and contribute to the mechanisms underlying AD. The present study used this multimodality approach to investigate, by means of a hybrid PET/MR scanner, the coupling between glucose consumption and intrinsic functional activity in 23 patients with AD-related cognitive impairment ranging from amnestic mild cognitive impairment (MCI) to mild-moderate AD (aMCI/AD), in comparison with a group of 23 healthy elderly controls. Between-group (Controls > Patients) comparisons were conducted on data from both imaging modalities using voxelwise 2-sample t-tests, corrected for partial-volume effects, head motion, age, gender and multiple tests. FDG-PET/fMRI relationships were assessed within and across subjects using Spearman partial correlations for three different resting-state fMRI (rs-fMRI) metrics sensitive to AD: fractional amplitude of low frequency fluctuations (fALFF) and regional homogeneity (ReHo) of rs-fMRI BOLD signal along with group independent component analysis with dual regression (gICA-DR). FDG and rs-fMRI metrics distinguished aMCI/AD from controls according to spatial patterns analogous to those found in stand-alone studies. Within-subject correlations were comparable across the three rs-fMRI metrics. Correlations were overall high in healthy controls ($\rho=0.80\pm0.04$), but showed a significant 17% reduction ($p<0.05$) in aMCI/AD patients ($\rho=0.67\pm0.05$). Positive across-subject correlations were overall moderate ($\rho=0.33\pm0.07$) and consistent across rs-fMRI metrics. These were confined around AD-target posterior regions for metrics of functional connectivity (ReHo and gICA-DR). In contrast, FDG/fALFF correlations were distributed in the frontal gyrus, thalami and caudate nuclei. Taken together, these results support the presence of bioenergetic coupling between glucose utilization and rapid transmission of neural information in healthy ageing, which is substantially reduced in aMCI/AD, suggesting that abnormal glucose utilization is in some way linked to communication breakdown among brain regions impacted by the underlying pathological process.

Keywords

Mild cognitive impairment, Alzheimer Disease, Fludeoxyglucose PET, Brain functional MRI, Intrinsic functional connectivity, Default mode network.

Highlights

- **Estimates of fluorodeoxyglucose metabolism and intrinsic functional activity and connectivity, simultaneously assessed under the same physiological condition, are both sensitive to aMCI/AD in impacted brain regions.**
- **The relationship between resting-state FDG-PET and BOLD-fMRI metrics is reduced in aMCI/AD patients by approximately 17% relative to healthy elderly controls.**
- **Metrics of resting-state fMRI connectivity and signal amplitude are related to fluorodeoxyglucose metabolism in different regions of the brain.**

1. Introduction

Alzheimer Disease (AD) is a chronic neurodegenerative disorder that affects approximately 9 million people in Europe (Diaz-Ponce et al., 2016). This disease is characterized by asymptomatic onset (Dubois et al., 2014) followed by cognitive decline that worsens with disease progression (Bouwman et al., 2010; McKhann et al., 1984). AD affects memory and the ability to carry out voluntary and purposeful actions, inducing difficulties in language production and comprehension as well as disorientation in time and space.

Novel biomarkers have been developed to support the diagnosis of AD (Dubois et al., 2014). These are primarily derived from structural magnetic resonance imaging (MRI) of the hippocampus (Sarazin et al., 2010) and from analysis of cerebral spinal fluid (CSF) amyloid β (Aβ) or tau protein concentrations (Nisbet et al., 2015; Nordberg, 2010). In addition, molecular neuroimaging biomarkers by means of positron emission tomography (PET) using ^{18}F-2-fluoro-2-deoxy-D-glucose (FDG-PET), which reflects glucose metabolism mainly from neurons (Dennis, 2014), provides an accurate predictor of AD progression in the form of temporo-parietal, posterior Cingulate and Precuneus hypometabolism (Chételat et al., 2003; Ito et al., 2015; Minoshima et al., 1997; Mosconi, 2005; Scheltens et al., 2016).

In these regions, resting-state functional MRI (rs-fMRI), which exploits the blood-oxygen level-dependent (BOLD) endogenous contrast (Buckner et al., 2008; Dennis, 2014; Greicius et al., 2004; Supekar et al., 2008), has disclosed the physiological presence of intrinsic functional architectural patterns in the low-frequency (0.01-0.1 Hz) oscillations, including the default mode network (DMN) (Gusnard et al., 2001), which are sensitive to the AD process (Greicius et al., 2004; Hafkemeijer et al., 2012; Klaassens et al., 2017; Zhang et al., 2010). rs-fMRI therefore has potential clinical relevance, especially as it is non-invasive, relatively inexpensive and easy to acquire in comparison to PET-FDG.

The recently developed hybrid PET/MRI scanners now allow one to simultaneously acquire glucose metabolism and rs-fMRI under the same physiological condition (Wehrl et al., 2015). This constitutes an exciting opportunity to investigate the relationships between intrinsic metabolic and functional brain changes (Aiello et al., 2016; Cecchin et al., 2017; Tahmasian et al., 2015). To date,

published studies that have integrated these two imaging modalities in a simultaneous acquisition setup have involved healthy adults using seed-based methods for rs-fMRI network analysis (Riedl et al., 2014), or healthy elderlies using local intrinsic functional activity metrics (Aiello et al., 2015). However, to date the intimate coupling between FDG-PET hypometabolic pattern and rs-fMRI network disruption in AD-related brain damage has been little addressed.

To the best of our knowledge, no simultaneous PET/fMRI study published to date has investigated how early AD-related local changes in resting-state glucose consumption relate to the changes in functional activity observed in stand-alone rs-fMRI studies. Such knowledge is likely to provide novel insights towards the development of clinically relevant tools (Drzezga et al., 2014; Tahmasian et al., 2015). In the present simultaneous resting-state FDG-PET/fMRI study we investigated the relationships between glucose consumption and intrinsic functional activity in healthy aged individuals and patients with mild AD on a voxel-by-voxel basis. Intrinsic functional activity was assessed by means of three metrics that differ in spatial-extent definition and relevance to AD process (Aiello et al., 2016; Cha et al., 2015; Damoiseaux et al., 2012), namely i) fractional amplitude of low frequency fluctuations (fALFF), a single-voxel indicator of BOLD signal frequency power independent from brain connectivity thereof (Zou et al., 2008; Zuo et al., 2010); ii) regional homogeneity (ReHo), a measure of local functional connectivity (Zang et al., 2004); and iii) group-independent component analysis with dual regression (gICA-DR), which identifies common spatiotemporal patterns and project them back to each individual (Beckmann et al., 2009; Beckmann & Smith, 2004).

2. Materials & Methods

2.1 Patient population

A total of twenty-three patients (**Table 1**) were recruited at the Istituto di Ricovero e Cura a Carattere Scientifico (IRCCS) SDN in Naples, Italy. Among them, seventeen were diagnosed with mild-to-moderate probable AD according to the National Institute on Aging and the Alzheimer's Association (NIA-AA) workgroup (McKhann et al., 2011) and six fulfilled the diagnostic criteria of amnestic MCI (Peterson et al., 2008). All AD patients had a typical clinical phenotype with predominant memory impairment without clinical/MRI features suggestive of primary progressive aphasia or posterior cortical atrophy. The whole group of the aMCI/AD patients underwent routine clinical and standard laboratory assessments, including a neurological examination and a neuropsychological evaluation, and a brain simultaneous resting-state FDG-PET/fMRI acquisition, followed by axial T2 fluid-attenuated inversion recovery (FLAIR), T2 turbo spin echo (TSE) and diffusion weighted imaging (DWI) acquisitions.

Patients received the clinical dementia rating (CDR) and a neuropsychological measurement of

global cognitive functioning (mini mental status examination (MMSE); Folstein et al., 1975) and the evaluation of memory, language, executive function/attention, and visuo-construction abilities. Exclusion criteria included a history of other neurologic or major psychiatric disorders and systemic diseases that may affect cognitive functions (e.g. uncontrolled endocrine disorder) and the presence of any significant cerebral focal lesion on brain MRI apart from mild age-related leukoaraiosis (Fazekas score <2) (Fazekas et al., 1987). Anti-cholinesterase (AChEI) and antidepressant drug therapies were not a cause for exclusion. In the whole group, 26% of the patients were treated with AChEI, 17% with antidepressant and 17% with both (**Table 1**)

Twenty-three healthy elderly already presented in our previous work (Aiello et al., 2015) were used as the control group and will herein be referred to as healthy elderly controls (**Table 1**). Exclusion criteria were the same as above. The local Institutional Review Board of the IRCCS SDN approved the study and informed written consent was obtained from all subjects.

2.2 Acquisition protocol

A Biograph mMR MR-PET integrated system (Siemens Healthcare, Erlangen, Germany) was used to simultaneously acquire rs-fMRI and FDG-PET data from the 3T MRI scanner and its embedded PET tomograph installed between the gradient and radio-frequency coils, respectively (Delso et al., 2011). Static FDG-PET data were acquired in sinogram mode for 15 minutes, matrix size was 256x256, including corrections for random coincidences, dead-time, scatter and photon attenuation, reconstructed with the ordered subset-expectation maximization (OSEM) algorithm (21 subsets, 4 iterations) and post-filtered with isotropic full-width half-maximum (FWHM) gaussian kernel of 4 mm. Attenuation correction was performed using MR-based attenuation maps derived from a dual echo (TE = 1.23-2.46 ms) Dixon-based sequence (TR = 3.60 ms), allowing for reconstruction of fat-only, water-only and of fat-water images (Aiello et al., 2015).

As FDG-PET acquisition started, clinical MRI sequences including three-dimensional T1-weighted magnetization-prepared rapid acquisition gradient-echo sequence (MPRAGE, 176 sagittal planes, 256×240 mm2 field of view, voxel-size 1×1×1 mm3, TR/TE/TI 2300/2.96/900 ms, flip angle 9°, TA = 5′14″) and T2*-weighted single-shot echo-planar imaging (EPI) sequence (voxel-size 4×4×4 mm3, TR/TE = 1920/32 ms, flip angle=90°, 240 time points, field of view (FOV) read=256, distance factor=0, TA=7′40″) were run consecutively.

In line with the procedure guidelines for PET brain imaging provided by the European Association of Nuclear Medicine (EANM) (Varrone et al., 2009), patients were asked to fast for at least 6 hours prior to FDG injection: approximately 250 MBq of 18F-FDG were intravenously injected only if glycaemia was below 120 mg/dl. Patients were positioned in a quiet and warm dark room 15 min before FDG administration and during the uptake phase. Simultaneous resting-state FDG-PET/MRI data

acquisition started 30 min following the injection of FDG. PET data were acquired in 15 minutes. While in the scanner, subjects were asked to relax, not to be engaged in structured thoughts and keep their eyes open to avoid falling asleep.

2.3 Data preprocessing

Imaging data were analyzed using Analysis of Functional NeuroImages (AFNI) 17.1.01 (Cox, 1996, 2012) and FSL 5.0.4 (Jenkinson et al., 2012; Smith et al., 2004) 64-bit software on a Mac-OS 10.7 computer. BOLD-weighted, anatomical MRI and FDG-PET images were preprocessed in each single-subject space (**Figure 1**). All Digital Imaging and Communications in Medicine (DICOM) images were anonymized and converted to compressed Neuroimaging Informatics Technology Initiative (NIfTI) format using the DCM2NII tool (https://www.nitrc.org/projects/dcm2nii).

T1-weighted images were skull-stripped using the Brain Extraction Tool (BET) with the robust brain centre estimation option, aligned to corresponding BOLD-weighted and FDG-PET images (3dAllineate, AFNI), resampled to 2 mm isotropic (3dresample, AFNI) to accommodate for EPI and FDG-PET resolution differences, and segmented into probabilistic grey matter (GM), white matter (WM) and CSF compartments (FAST, FSL). Individual GM binary masks were thus derived from 50% GM suprathresholded voxels plus those whose GM probability exceeded those of WM and CSF, respectively (3dcalc, AFNI). Probabilistic weighted GM density maps were then coregistered to the MNI-ICBM-152 stereotaxic template using 12 degrees-of-freedom (DOF) affine transformations (flirt, FSL). The affine transformation matrix was used to conduct a non-linear spatial normalization of the T1-weighted image (fnirt, FSL), and weighted GM density maps were finally warped to the MNI template using non-linear registration parameters (applywarp, FSL). The cerebellum was excluded from any GM density maps due to its partial coverage in BOLD-EPI sequences.

FDG-PET images were skull-stripped using BET with bias-field and neck cleaned-up (Jenkinson et al., 2005; Smith, 2002). Images were masked within the corresponding individual GM binary mask in the single-subject space (3dcalc, AFNI) and then spatially normalized to the MNI stereotaxic template (Grabner et al., 2006) using the non-linear transformation parameters (applywarp, FSL), resampled at 2-mm isotropic (3dResample, AFNI) voxels and standardized to z-scores with respect to FDG mean and standard deviation across GM voxels (3dcalc, AFNI). Moreover, the standardized uptake value ratio (SUVR) was also calculated by global mean normalization, as commonly evaluated in ^{18}F-FDG PET studies of aMCI/AD.

Preprocessing of BOLD-weighted images included the removal of first 10 volumes to avoid non-equilibrium magnetization effects (fslroi, FSL), head motion (mcflirt, FSL) and slice-timing (slicetimer, FSL) corrections, non-brain tissue removal (BET, FSL). Multiple linear regressions of the 6 head motion displacements plus their derivatives and mean WM and CSF timeseries were applied to remove

additional sources of spurious physiological noise (3dDeconvolve, AFNI). Linear and quadratic trends were also removed at this stage. Then, the temporal mean image was re-added to the residual volumes in a voxel-wise fashion.

2.4 rs-fMRI metrics

Neural activity is associated with low-frequency spontaneous BOLD oscillations. For this reason, each subject's BOLD-EPI image ratio from within the low-frequency range (0.01-0.1 Hz) out of the total power spectrum, referred to as fractional amplitude of low frequency fluctuations (fALFF), was calculated within each individual GM binary mask on a voxel-by-voxel basis (3dRSFC, AFNI). Afterwards, each subject's BOLD-EPI image was temporally filtered (0.01-0.1Hz) using a bandpass filter (fslmaths, FSL) to allow the estimation of rs-fMRI connectivity metrics. Then, ReHo maps were defined as metrics of local functional connectivity. These were estimated calculating the Kendall's coefficient of concordance (Kendall & Gibbons, 1990) in clusters of 27 nearest-neighborhood voxels across the entire brain (3dReHo, AFNI) within each individual GM binary mask.

Thereafter, individual BOLD-EPI images, fALFF and ReHo maps were spatially smoothed using a 6-mm FWHM gaussian kernel (3dFWHMx, AFNI) that emulates the resulting smoothing applied to FDG-PET maps, spatially normalized to stereotaxic space using the non-linear transformation parameters (applywarp, FSL), resampled at 2-mm isotropic voxels and standardized to z-scores with respect to each metric's GM mean and standard deviation, respectively (3dcalc, AFNI).

In addition to local intrinsic brain functional metrics, large-scale intrinsic functional connectivity was calculated using gICA-DR across all individuals (N=46) using the temporal-concatenation procedure implemented in the Multivariate Exploratory Linear Optimized Decomposition into Independent Components (MELODIC) from the FSL library (Jenkinson et al., 2012). The concatenated BOLD-weighted data were variance-normalized to account for temporal dynamics in each voxel timeseries and decomposed into 15 independent components. This dimensionality allowed optimal IC estimation and minimized splitting effects (Abou Elseoud et al., 2011; Marchitelli et al., 2017).

Among these 15 components, we identified the component corresponding to the DMN using an in-house automated spatial overlapping procedure (3dcalc, AFNI) between each component and a DMN template (Yeo et al., 2011). The suprathresholded ($z>3.2$) component with the highest number of overlapping voxels and the lowest of non-overlapping voxels related to the template was selected and projected back onto each preprocessed individual BOLD-weighted image using the dual-regression methodology as implemented in FSL and finally standardized to z-scores as the other rs-fMRI metrics (3dcalc, AFNI).

2.5 Head movement

Metrics of intrinsic functional activity are known to be highly sensitive to head movements (Power et al., 2012). In particular, healthy elders and patients typically show higher and more heterogeneous head motion profiles than healthy young adults. We have therefore measured the amount of head movements from the six timeseries of head motion displacement obtained after head motion correction of rs-fMRI data to rule out the possibility that motion could compromise metrics of intrinsic brain activity for a particular subject and hamper the comparison between the two samples.

In particular, timeseries indicating rotations were converted to millimeters, considering a sphere of radius 50 mm as the best estimate of the mean distance from the cerebral cortex to the center of the head. The derivative of each motion displacement timeseries was then calculated. The straight sum across the absolute derivative timeseries was calculated to yield a single framewise displacement (FD) timeseries (n=230) that summarized instantaneous movements in each subject (Power et al., 2012). Furthermore, the temporal median of FD timeseries was calculated to summarize motion per each subject. This choice depended upon the greater robustness of median values against outliers, and to account for non-normally distributed FD timeseries samples.

2.6 Between-group comparisons

In this study, statistical analyses of scalar quantities were assessed using IBM SPSS Statistics v22, whereas voxel-based statistical evaluations were conducted in AFNI. The statistical significance level was set to $p<0.05$ corresponding to $z>1.96$.

A chi-squared test was conducted to assess between-sample gender effects whereas independent 2-sample t-tests were conducted to evaluate whether mean age, MMSE scores and temporal median FD values were statistically different between healthy elderly controls and aMCI/AD patients. Independent 2-sample t-tests were also conducted on full individual datasets on a voxel-by-voxel basis (3dttest++, AFNI) across the two groups (healthy>AD) for each imaging modality and metric (FDG-PET, fALFF, ReHo, gICA-DR). Since head movements (Power et al., 2012) and GM atrophy (Xie et al., 2015) likely bias these comparisons, median individual FD values were included together with age and gender as group scalar covariates. Furthermore, probabilistic GM maps were also included as voxel-based covariates to deal with the variability in GM density across groups. Statistical t-maps were standardized to z-scores and further corrected for false positive clusters (3dClustSim, AFNI), applying the alphasim method option (3dttest++, AFNI). This option computes sign-randomization and permutation (N=10000) of the t-test statistic residuals to generate null-hypothesis datasets. Then, significant clusters were defined considering a 1-sided threshold and first-nearest neighbor clustering methods. The per-cluster statistical significance level was set to $p<0.05$ and false positive rate significance threshold to $\alpha<0.05$. The dual approach proposed by Poldrack et al., 2017 was adopted to minimize type II errors. The voxelwise unthresholded z-scores maps will be shared through the NeuroVault repository

(https://neurovault.org) for visualization, downloading and further usage in meta-analysis studies. Spearman's rank correlations (ρ) were calculated between individual median brain functional/molecular metrics and corresponding median FD values to assess relationships with motion.

2.7 Within-subject PET/fMRI correlations

To assess the relationship between resting-state FDG-PET and fMRI-based metrics, within-subject PET/fMRI partial correlations were calculated voxel-by-voxel in Matlab R2017b. After preprocessing and standardization into z-scores, individual FDG, GM probability and fALFF, ReHo and gICA-DR 3D images were linearly converted into 1D column vectors (3dmaskdump, AFNI). For each subject (N=46), Spearman rank correlations between FDG-PET and each separate fMRI-based metric dataset were conducted, partialling out GM probability values to minimise unwanted structural atrophy-induced biases. Corrections for multiple comparisons were conducted using the Bonferroni method ($p < 0.02$).

A Friedman test was conducted to either assess differences among PET/fMRI metrics or evaluate group effects. Multiple comparisons were conducted using Bonferroni's correction in the former case only, as the latter involved less than three tests. For each FDG/fMRI metric correlation, the effect sizes were reported with respect to the two groups. These were calculated using the Cohen's d formula (Cohen, 1988) and corrected for bias using Bessels' correction (McGrath and Meyer, 2006).

2.8 Across-subject PET/fMRI correlations

Across-subject correlations were calculated in AFNI. For each imaging modality and metric, volumes were concatenated across all subjects and patients (N=46) (3dTcat, AFNI). The choice of concatenating all subjects from both groups relies on the assumption that neural specificity increases when considering both groups together, besides the advantage of the larger sample size (Aiello et al., 2015). To reduce across-subject GM variability biases, those voxels present in less than 45/46 subjects were excluded. Afterwards, Spearman's rank across-subject correlations were calculated between FDG-PET and each rs-fMRI metric, within each GM voxel (3dTcorrelate, AFNI) adjusting for partial volume effects (Altman, 1991). Scalar covariates were not included in this analysis given that they showed no significant effect in any voxel between the two groups.

In order to evaluate the presence of differences in across-subject FDG/fMRI correlational patterns according to the rs-fMRI metric considered, the procedure above was repeated using a bootstrap resampling strategy for each single subject (N=46) for a total sample of N=47. The paired voxelwise Friedman test was then conducted to identify the three highest-ranked regions associated with each FDG/fMRI correlational metric on the whole brain (3dFriedman, AFNI). In each region identified, multiple comparisons were conducted using paired post-hoc 2-sample t-tests on the entire sample (N=47) between the highest-ranked FDG/fMRI correlation metric for that region versus the other correlation metrics. Results were Bonferroni corrected.

3. Results

3.1 Between-group analyses

There was a significant difference in mean age (dof=38, t=-3.04, p=0.004 by independent two-sample t-test, adjusted for unequal variance), and gender distributions (z=4.73, p<0.01, CI = 0.07-0.63) between neurologically healthy controls and aMCI/AD patients. There was also a statistical difference in mean MMSE (dof=24.6, t=-7.3, p<0.001 by independent two-sample t-test, adjusted for unequal variance) between the two samples in question (**Table 1**). We found low estimates of head movements across healthy subjects and patients, without significant between-group difference (0.06±0.08mm and 0.09±0.24mm, respectively; dof=29.3, t=-1.5, p=0.15 by independent two-sample t-test, adjusted for unequal variance). Non-significant correlations were found between median FD timeseries and the median intrinsic brain activity metrics from both PET and fMRI modalities across all subjects.

Results from the voxelwise independent t-test between healthy elderly controls and aMCI/AD are shown in **Figure 2** and summarized in **Table 2** for each metabolic and functional variable. Results are herein reported for z-scores standardized FDG-PET data only, since the FDG-PET SUVR data yielded similar results. In patients, significant FDG hypometabolism was found in posterior and anterior cortical regions, with a symmetric pattern across hemispheres. Three major clusters were found in posterior regions, centered on the Precuneus and right and left Superior Temporal gyri (STG). The Precuneus cluster encompassed portions of the Cuneus and the Posterior Cingulate Cortex (PCC) in both hemispheres. The clusters centered on the STG extended into the Inferior Parietal Lobule (IPL), the Angular and Supramarginal gyri, and into the Middle Temporal gyrus (MTG) up to the Fusiform gyrus in both hemispheres. One cluster was found in the medial prefrontal cortex, centered on the medial part of the Superior Frontal gyrus (SFG), extending into superior frontal areas, neighboring the Anterior Cingulate Cortex (ACC). These clusters all survived a more stringent cutoff (p<0.01), with only the Precuneus cluster surviving the p<0.001 thresholding. A hypometabolic cluster also involved the thalami and lentiform and caudate nuclei, although it did not survive the p<0.01 cutoff. Regarding covariates, no significant cluster associated with age, gender, head motion or GM atrophy exceeded the false positive clustering threshold (α>0.05).

In aMCI/AD, rs-fMRI metrics all showed significant changes in signal amplitude and disruption of intrinsic functional connectivity. In general, they consisted in symmetric clusters across both hemispheres and all involved the PCC and Precuneus (**Figure 2**, **Table 2**). Besides these regions, significant fALFF alterations mostly involved the SFG, contrasting with ReHo, which did not affect anterior brain regions. Two additional posterior ReHo clusters centered on the right Supramarginal and left Angular gyri, the latter encompassing also the Supramarginal gyri, the IPL and portions of the STG.

Finally, gICA-DR did not involve any other region over and above the Precuneus/PCC. The fALFF and gICA-DR clusters did not survive the p<0.01 thresholding, while the ReHo right Supramarginal gyrus did, but not to more stringent ones. Regarding covariates, no cluster associated with age, gender, head motion or GM atrophy exceeded the AlphaSim threshold differentiating healthy aged controls from aMCI/AD patients, for any rs-fMRI metric.

To summarize the above findings, hypometabolic regions were largest and as expected located mainly in posterior brain regions. rs-fMRI changes consistently involved the PCC/Precuneus across all three metrics, with gICA-DR showing the least number of clusters. Over and above this consistent finding across metrics, fALFF and ReHo showed additional dysfunctional areas with opposite anterior/posterior patterns, namely ReHo displayed posterior association cortex involvement close to that observed with FDG, and fALFF anterior frontal involvement.

3.2 Within-subject PET/fMRI correlations

Figure 3 depicts the FDG-rs-fMRI correlations for each subject. Significant Spearman correlations were found in all subjects. The correlations ranged from moderate to high and were statistically consistent across rs-fMRI metrics (FDG/fALFF: 0.59-0.88; FDG/ReHo: 0.59-0.86; FDG/gICA-DR: 0.60-0.87). In fact, there were no statistically significant differences among resting-state FDG-PET/fMRI correlations according to the fMRI metric considered ($\chi^2(2) = 3.7$; $p = 0.16$).

In contrast, there were statistically significant differences in correlational values between the two groups of healthy old individuals and aMCI/AD patients ($\chi^2(1) = 69$; $p < 0.001$). Regarding the FDG/fALFF relationship, the mean correlation coefficient was significantly lower in patients versus healthy controls (ρe 0.67±0.04 and 0.80±0.04, respectively; dof=44, t=9.9, p<0.001 by independent two-sample t-test), for an absolute percent change of 17.4%. The effect size scored 2.95, indicating that individual FDG/fALFF correlations allow identification of aMCI/AD patients at approximately 91% (range: 89–93%) probability, with only a 4% chance that a random aMCI/AD patient would score higher than neurologically healthy individuals.

Similar findings applied to the FDG/ReHo (ρ=0.66±0.05 and 0.79±0.04, respectively; dof=44, t=10, p<0.001), showing a 18.1% reduction in aMCI/AD patients. The effect size score was identical to that found for FDG/fALFF. Lastly, the FDG/gICA-DR relationships (ρ=0.68±0.04 and 0.79±0.04, respectively; dof=44, t=9.1, p<0.001) were similarly reduced by 15.1%. The effect size scored 2.68, which indicates that individual FDG/gICA-DR correlations allow identification of aMCI/AD patients at nearly 89% (range: 89–93%) probability, with a 7% chance that a random aMCI/AD patient would score higher than neurologically healthy individuals.

In summary, significant and positive FDG-rs-fMRI correlations were present in every single subject, control or patient, examined, and for all three rs-fMRI metrics. The coupling strength was also

consistent across rs-fMRI metrics, and consistently lower by approximately 17% in aMCI/AD relative to controls.

3.3 Across-subject PET/fMRI correlations

Voxelwise resting-state FDG-PET/fMRI Spearman correlations across subjects are shown in **Figure 4** and summarized in **Table 3**. FDG/fALFF correlations were on average moderate (ρ=0.34±0.08), involving only 9% of total GM voxels after partial volume correction. Clusters of significant positive correlations were overall modest in size and symmetrically distributed across hemispheres. The spatial overlap between these clusters and group hypo-metabolic areas present in aMCI/AD was 56.5%, within which the magnitude of correlations was similar to the mean (ρ=0.33±0.07). The strongest correlations centred in the Caudate nucleus, Thalamus and mid-cingulate gyrus. Other prominent clusters involved parts of the MFG and SFG, while a small cluster involved the IPL. No correlations involved the Precuneus and PCC.

FDG/ReHo correlations were also moderate (ρ=0.33±0.07) covering 7% of total GM. Major clusters involved the PCC, the mid-cingulate, Precuneus and temporo-parietal areas. These spatial patterns were symmetrical across hemispheres and yielded an overall 65.3% overlap with hypometabolic aMCI/AD regions, with similar average correlation coefficients (ρ=0.34±0.07).

FDG/gICA-DR correlations were similarly moderate (ρ=0.33±0.07), covering 8% of total GM volume. The largest cluster centered on the PCC and Precuneus, followed by other posterior association regions including the Supramarginal, Angular and Superior Temporal gyri. Clusters were also found in anterior cortical areas within the MFG. They were of similar magnitude inside the 71% overlap with the hypometabolic aMCI/AD regions (ρ=0.33±0.07).

Multiple comparisons across PET/fMRI metrics corroborated the above findings and are reported in **Table 4**. Paired t-tests involving FDG/fALFF revealed statistically significant increased correlations in both Middle Frontal gyri and the left Superior Medial Frontal gyrus when compared with FDG/ReHo and FDG/gICA-DR alike.

Those involving FDG/ReHo revealed statistically significant increased coupling in the Angular gyri and right Inferior Frontal gyrus when compared with both FDG/fALFF and FDG/gICA-DR. Furthermore, no statistically significant increased correlations were detected between FDG/ReHo and FDG/gICA-DR in the PCC, although such an increase was observed for FDG/gICA-DR when compared to FDG/fALFF correlations only.

In summary, across-subject resting-state FDG-PET/fMRI correlations in this cohort of healthy elderly controls and aMCI/AD patients were consistently moderately strong for all three rs-fMRI

metrics. These were located around the DMN regions for the two functional connectivity metrics, namely ReHo and gICA-DR, whereas regarding the signal amplitude metric fALFF, they were distributed anteriorly in frontal gyri, and involved the thalamus and caudate nucleus as well.

4. Discussion

In this study, we have evaluated the relationships between the brain's glucose consumption and metrics of intrinsic neural activity in healthy elderly subjects and aMCI/AD patients thanks to simultaneously acquired resting-state FDG-PET/fMRI data. Our main findings can be summarized as follows:

1. Metrics from both imaging modalities are sensitive to process and reveal a predominant posterior cortical involvement typical of aMCI/AD. While FDG-PET differentiated aMCI/AD patients from healthy controls in most of the DMN, rs-fMRI metrics were able to identify patients in fewer DMN cortical regions. Notwithstanding, all metrics converged in the PCC.
2. The resting-state FDG-PET/fMRI correlation examined within each subject is high in the healthy elderly ($\rho \approx 0.8$) and reduced by about 17% in aMCI/AD, an effect consistent in the correlation with the three rs-fMRI metrics.
3. The resting-state FDG-PET/fMRI correlations examined across subjects revealed overall few moderately strong positive correlations, spatially distributed mostly around the DMN or hypometabolic areas. FDG/gICA-DR showed highest overlap around posterior DMN nodes, whereas FDG/fALFF showed lowest overlap, with anterior distribution and involving additional non-DMN regions such as the thalamus and caudate nucleus.

In agreement with stand-alone studies, both resting-state FDG-PET and rs-fMRI metrics were able to distinguish a group of amnestic MCI and mild-to-moderate AD patients from healthy similarly aged controls on a voxel-by-voxel basis. Consistent with the literature, these findings from both imaging modalities reflect a failure in neuronal integration and signaling in these patients, particularly converging around the Precuneus and PCC (Badhwar et al., 2017; Cha et al., 2015; Klaassens et al., 2017).

FDG hypometabolism in aMCI/AD was prevalent in DMN regions (Brown et al., 2014) and larger in spatial extent as compared to patterns of altered functional activity and hypo-connectivity derived from rs-fMRI. This could reflect basic physiological differences between FDG and BOLD signal: the former capitalizes on high stable signal reflecting regionally variable levels of resting-state glucose utilization (Fox et al., 1988) experiencing little or no physiological artifacts, whereas the latter has low intrinsic signal that arises from hemodynamic mechanisms in relation to oxygen consumption (Hyder et al., 2016), which can be affected by in-scanner drowsiness or physiologically altered conditions (Huang et al., 2017, Algarin et al., 2017 Zhou et al., 2017). The differences could also arise

from BOLD-related confounding factors such as head movements, cardiac/respiration cycles, and unstable arterial pressure of carbon dioxide (pCO_2) and blood pressure. These factors, albeit mitigated by data preprocessing, can bias metrics of BOLD signal amplitude and functional network connectivity. However, it should be noted that regional patterns of alterations such as those found in our patient group are unlikely to be generated by these confounding factors, which are more likely to induce distributed effects across the whole brain.

Across metrics, rs-fMRI was able to differentiate aMCI/AD from healthy controls in DMN regions. This finding is in agreement with the literature reporting accelerated reduction of intrinsic DMN activity in early AD (Dennis & Thompson, 2014). Interestingly, rs-fMRI metrics only partially agreed with respect to the regional characterization of aMCI/AD. Although all metrics identified aMCI/AD in the PCC node, only fALFF differentiated aMCI/AD patients in the medial prefrontal cortex, whereas only ReHo did so in the temporo-parietal regions of the DMN. This suggests that the three fMRI-based metrics of intrinsic activity and connectivity assessed here have differential sensitivity to the functional isolation of the DMN subsystems, which itself may result from non-local structural disconnection or from differential degrees of regional amyloid deposition (Chetelat et al., 2009; Montembeault et al., 2016).

Our findings also support the gICA-DR method and associated large-scale brain networks. This approach enabled us to identify neuronal DMN patterns in each subject from an unique ICA procedure, facilitating the comparison of the two populations (Calhoun & Adali, 2012). Our gICA-DR findings are in line with previous work showing that the PCC and Precuneus are directly involved in AD-related neurodegeneration (Binnewijzend et al., 2012; Greicius et al., 2004). Compared with ReHo, gICA-DR did not reveal the involvement of temporo-parietal DMN regions in aMCI/AD. This discrepancy might be associated to different computational procedures across rs-fMRI methods. In the particular case of gICA-DR, the method provides for a single spatial group DMN component which represents common spatiotemporal traits across all subjects involved in this study (Calhoun & Adali, 2012; Liu et al., 2008; Smitha et al., 2017). It might also be that this discrepancy across the two functional connectivity methods relates to the greater specificity of DMN maps defined via gICA-DR methods. In fact, while DMN regions are characterized by greater signal intensity, non-DMN regions are dominated by noise (Beckmann et al., 2009).

Some have recently questioned the effectiveness of partial volume correction in healthy aging and aMCI/AD patients due to lack of sufficient evidence of an association between functional connectivity and GM volume density (Damoiseaux et al., 2017). Even though a structure/function association has yet to be determined in fMRI connectivity studies, partial volume correction remains an important statistical choice for both FDG-PET and rs-fMRI metrics in geriatric populations. The effectiveness of partial volume correction using structural information derived from high-resolution T1-

MPRAGE sequences has been demonstrated on FDG-PET (Chételat et al., 2008; Quarantelli et al., 2004; Shidahara et al., 2009;) and is systematically adopted in resting-state FDG/fMRI studies of aMCI/AD patients (Kazemifar et al., 2017).

We found high within-subject correlations between FDG-PET and all three rs-fMRI metrics in healthy aged individuals. This suggests fine-tuning of cortical glucose utilisation with neurovascular mechanisms physiologically related to neural activity (Mergenthaler et al., 2013). This finding is in agreement with, and generalizes previous resting-state FDG-PET/fMRI correlational studies of neurologically normal aged subjects (Aiello et al., 2015; Kazemifar et al., 2017, Bernier et al., 2017).

We also found significantly reduced within-subject correlations in aMCI/AD. This finding agrees with a recent non-simultaneous resting-state FDG-PET/fMRI study of probable AD patients from the Alzheimer's Disease Neuroimaging Initiative (ADNI) dataset (Kazemifar et al., 2017). Compared to this earlier report, the present study revealed overall lower correlations. This might reflect differences in disease stage between the two studies, i.e., more advanced in ours, suggesting worsening of the glucose/oxygen molecular coupling or inadequate glucose-mediated regulation of cerebral blood flow with disease progression (Mergenthaler et al., 2013).

Reduced within-subject FDG-PET/fMRI correlations in aMCI/AD might represent a chronic inability of perfusion to adjust to glucose metabolism, which has been speculated by some to lead to brain hypo-perfusion and from there to neurodegeneration (Nicolakakis & Hamel, 2011). Besides, oxidative and bioenergetic stress alter neurovascular processes, which may also lead to neurodegeneration (Harris et al., 2012; Kapogiannis & Mattson, 2011; Nicolakakis & Hamel, 2011). These include alterations in the glucose-selective permeability of the blood-brain barrier or malfunctioning of glucose transporter 3 (GLUT3), in turn affecting delivery of energetic fuels to neurons, especially when distant from capillaries (Simpson et al., 2007).

In bioenergetic terms, our results suggest that glucose metabolic impairments in mild AD might lead to insufficient resources to cover the nerve cells' needs for chemical syntheses, transport and signaling. This imbalance might in turn reduce the efficiency and economy of neural information processing, affecting even more complex intrinsic brain functional systems, from regional microcircuits to large-scale networks (Kapogiannis & Mattson, 2011).

The findings from the across-subject correlational analysis support the bioenergetic hypothesis. Indeed, local functional connectivity (i.e. ReHo) correlated to FDG in the DMN, a finding further supported by the large-scale functional connectivity (i.e. gICA-DR) analysis. In fact, ReHo presented a significantly increased FDG-coupling in temporo-parietal regions of the DMN, while gICA-DR revealed a significant increase in FDG-coupling in posterior DMN nodes. This network is characterized by exacerbated changes in aMCI/AD compared to healthy aged subjects (Jones et al., 2011). It is worth

noting that in our previous investigation involving healthy aged individuals (Aiello et al., 2015), correlations were weaker and not distributed around DMN regions. It is likely that adding amnestic MCI and mild-moderate AD subjects in the correlational analysis increased the variance in multimodal imaging metrics and in turn the strength of the FDG-PET/fMRI correlations, given the systematic DMN hypometabolism and hypo-activation present in the clinical cohort. Overall, therefore, our present findings speak in favor of the development of PET-informed rs-fMRI classification of dementia (Rahim et al., 2015), including the adoption of data-based functional connectivity methods and definition of priors from simultaneously acquired data.

The spatial distributions of across-subject FDG/fALFF correlations highlighted the prefrontal cortex and the Supramarginal gyrus, but did not include the PCC and Precuneus where the coupling was significantly reduced compared to FDG/gICA-DR. Compared with other rs-fMRI metrics, significant increases in coupling were observed in both Middle Frontal gyri and left Superior Medial Frontal gyrus. The interpretation of this finding is difficult and speculative only. Compensatory mechanisms, in particular in the prefrontal cortex, might underlie increased glucose/oxygen coupling to protect memory function in aMCI/AD (Yap et al., 2017; Vemuri et al., 2012; Damoiseaux et al., 2012). Since perfusion impairment is unrelated to GM atrophy, whose effect was here removed using GM local volumes as covariates (Bozzao et al., 2001), the absence of correlation in the PCC and Precuneus as observed in FDG/fALFF across subjects might reflect increased oxygen demands in regions with severe hypo-perfusion possibly due to concomitant alterations of microvasculature as suggested by mild oxygen extraction fraction increase in temporo-parietal cortex in AD (Nagata et al., 2000). In future simultaneous PET/MRI studies, the acquisition of quantitative PET information from vascular transit time, vascular reactivity, and oxygen extraction fraction will better clarify the role of the FDG/fALFF relationship and its potential to monitor those compensatory mechanisms that characterize only those amnestic MCI individuals who are converting to AD (Nagata et al., 2002).

Across-subject resting-state FDG-PET/fMRI correlations might therefore suggest differential sensitivity among rs-fMRI metrics to pathophysiological mechanisms of AD. These metrics would rely to some degree on different hemodynamic components of the BOLD signal, which in turn determines slightly different spatial distributional FDG-PET/fMRI patterns. In the context of aMCI/AD individuals, fALFF might to some extent rely on perfusional mechanisms (Austin et al., 2011), whereas ReHo and gICA-DR would mostly rely on aerobic glycolysis (Bullmore & Sporns, 2012; Vaishnavi et al., 2010). Molecular approaches measuring the rates of cerebral oxygen and glucose metabolic consumption plus quantification of cerebral blood flow in AD patients would be useful to address these issues. An interesting issue that should be addressed in future studies using larger and homogeneous patient samples would be the relevance of fMRI/FDG coupling strength for the clinical/cognitive aspects of the disease.

This study has some limitations. First, we did not use cerebellar regions to normalize individual FDG and rs-fMRI metrics because of reduced FOV in BOLD-EPI sequences, and we normalized the data using mean individual GM as a reference region. While this choice might not be optimal, we did not however normalize the imaging data for the global cerebral mean, which has been shown to underestimate direct effects of aMCI/AD pathology in critical regions involved in the disease (Yakushev et al., 2007; 2008).

Second, neurologically healthy old controls and aMCI/AD patients differed in both age and gender. We added these as covariates to minimize any potential effects and explored voxelwise the location and extent of their effects across the two groups. Although no statistically significant effect was observed in the covariates, these imbalances may still have influenced the observed results owing to the previously reported effects of ageing on rs-fMRI connectivity (Goldstone et al., 2016). Notably, we conducted data preprocessing in individual native space and examined within-subject correlations, which should have overcome any such untoward effect. Also, we used data-driven methods to estimate global functional connectivity patterns and avoided the challenge of evaluating individual seed location shifts resulting from network reorganization (Goldstone et al., 2016). Our inability to select an a-priori seed prevented us from using a graph-theory approach. Furthermore, because gender exerts global effects on the functional and structural connectome (Goldstone et al., 2016), we limited our investigations to reduced connectivity in the DMN even though compensatory mechanisms may also affect other rs-fMRI networks in early aMCI/AD (Agosta et al., 2012). The underlying pathophysiological mechanisms require further investigation from a simultaneous molecular/functional imaging perspective.

Thirdly, in this study a number of scanned patients were treated with antidepressants. Specific chronic effects of these agents on regional FDG uptake or BOLD signal have not been clearly documented in healthy subjects and/or AD to our knowledge. Most part of available data is on acute challenge or short-term treatment in healthy subjects (Goldberg et al., 2004; McCabe & Mishor, 2011) and/or chronic therapy in patients with major depressive syndrome (Drevets et al., 2002). Also several patients were under AChEI, which have been shown to have different effects on cerebral glucose consumption and blood flow in young normals, aged normals, and Alzheimer's disease patients. Glucose metabolism was similarly reduced in almost all brain regions with a larger decrease in frontal cortex and in AD patients (Blin et al., 1997). Given treatment with these agents is commonplace in AD, it was considered unrealistic to exclude such patients if a sufficiently large sample was to be recruited for meaningful interpretation. On the other hand, our sample represents the usual AD population seen in memory clinics.

Another clinical limitation is the heterogeneity of the patient sample in disease severity and staging. However, our findings should mostly reflect mild AD since this category was predominant in the sample (15/23) although biomarkers of the pathophysiological process of AD (i.e. CSF and/or PET

biomarkers of brain amyloid-beta (Aβ deposition) were not included in the diagnostic criteria. Moreover the main aim of the present study was to assess the correlation between resting-state FDG-PET and BOLD-fMRI metrics at an individual level. Studies in larger samples of patients in whom the clinical diagnosis will be integrated with AD-biomarkers are required to assess the sensitivity of both modalities in detecting changes in AD at different stages of the disease and in particular in prodromal AD.

5. Conclusions

Effective neuroenergetic coupling of glucose/oxygen molecular utilization under homeostatic auto-regulated perfusional conditions is fundamental for neural signaling and interneuronal communication. This relationship is variable across subjects but well preserved in neurologically healthy ageing under physiological resting conditions. In contrast, it loosens with glucose hypometabolism consequent to aMCI/AD. Neuroenergetic disruption appears to impact different levels of brain functional organization, as observed by rs-fMRI, from BOLD signal amplitude in single voxels to regional microcircuits and large-scale functional networks in GM. By integrating FDG-PET and fMRI, this study documents differences in correlational patterns across rs-fMRI metrics ascribable to their degree of dependency on different BOLD hemodynamic components and their involvement, as well as allows for new insights into the pathophysiology of aMCI/AD.

Acknowledgements

This work was supported in part by Italian Ministry of Health (Current Research Projects). Funding by the European Union's Seventh Framework Programme (FP7/2007-2013, Grant Agreement No. HEALTH-F2-2011-278850 - INMiND), and by the CNR Strategic Project "The Aging: Technological and Molecular Innovations Aiming to Improve the Health of Older Citizens" is also gratefully acknowledged.

References

Agosta, F., Pievani, M., Geroldi, C., Copetti, M., Frisoni, G. B., Filippi, M. (2012). Resting state fMRI in Alzheimer's disease: beyond the default mode network, Neurobiology of Aging, 33, Issue 8, 1564-1578,

Aiello, M., Cavaliere, C., & Salvatore, M. (2016). Hybrid PET/MR imaging and brain connectivity. Frontiers in neuroscience, 10.

Aiello, M., Salvatore, E., Cachia, A., Pappatà, S., Cavaliere, C., Prinster, A., Nicolai, E., Salvatore, M., Baron, J-C., & Quarantelli, M. (2015). Relationship between simultaneously acquired

resting-state regional cerebral glucose metabolism and functional MRI: a PET/MR hybrid scanner study. Neuroimage, 113, 111-121.

Algarin, C., Karunakaran, K. D., Reyes, S., Morales, C., Lozoff, B., Peirano, P., Biswal, B. (2017 Mar 7). Differences on Brain Connectivity in Adulthood Are Present in Subjects with Iron Deficiency Anemia in Infancy. Front Aging Neurosci, 9:54.

Altman, D. G. (1991). Practical Statistics for Medical Research Chapman & Hall London Google Scholar.

Austin, B. P., Nair, V. A., Meier, T. B., Xu, G., Rowley, H. A., Carlsson, C. M., Johnson, S. C., & Prabhakaran, V. (2011). Effects of hypoperfusion in Alzheimer's disease. Journal of Alzheimer's Disease, 26(s3), 123-133.

Badhwar, A., Tam, A., Dansereau, C., Orban, P., Hoffstaedter, F., & Bellec, P. (2017). Resting-state network dysfunction in Alzheimer's disease: A systematic review and meta-analysis. Alzheimer's & Dementia: Diagnosis, Assessment & Disease Monitoring, 8, 73-85.

Beckmann, C. F., Mackay, C. E., Filippini, N., & Smith, S. M. (2009). Group comparison of resting-state FMRI data using multi-subject ICA and dual regression. Neuroimage, 47(Suppl 1), S148.

Beckmann, C. F., & Smith, S. M. (2004). Probabilistic independent component analysis for functional magnetic resonance imaging. IEEE transactions on medical imaging, 23(2), 137-152.

Bernier, M., Croteau, E., Castellano, C. A., Cunnane, S. C., Whittingstall, K. (2017 Apr 15). Spatial distribution of resting-state BOLD regional homogeneity as a predictor of brain glucose uptake: A study in healthy aging. Neuroimage.;150:14-22.

Binnewijzend, M. A., Schoonheim, M. M., Sanz-Arigita, E., Wink, A. M., van der Flier, W. M., Tolboom, N., Adriaanse S. M., Damoiseaux, J., Scheltens, P., van Berckel, B. N. M., & Barkhof, F. (2012). Resting-state fMRI changes in Alzheimer's disease and mild cognitive impairment. Neurobiology of Aging, 33(9), 2018-2028.

Blin, J., Ivanoiu, A., Coppens, A., De Volder, A., Labar, D., Michel, C., Laterre, E. C. (1997 Nov). Cholinergic neurotransmission has different effects on cerebral glucose consumption and blood flow in young normals, aged normals, and Alzheimer's disease patients. Neuroimage, 6(4), 335-43.

Bouwman, F. H., Verwey, N. A., Klein, M., Kok, A., Blankenstein, M. A., Sluimer, J. D., Barkhof, F., van der Flier, W. M., & Scheltens, P. (2010). New research criteria for the diagnosis of Alzheimer’s disease applied in a memory clinic population. Dementia and geriatric cognitive disorders, 30(1), 1-7.

Bozzao, A., Floris, R., Baviera, M. E., Apruzzese, A., & Simonetti, G. (2001). Diffusion and perfusion MR imaging in cases of Alzheimer's disease: correlations with cortical atrophy and lesion

load. American Journal of Neuroradiology, 22(6), 1030-1036.

Brown, R. K., Bohnen, N. I., Wong, K. K., Minoshima, S., & Frey, K. A. (2014). Brain PET in suspected dementia: patterns of altered FDG metabolism. Radiographics, 34(3), 684-701.

Buckner, R. L., Andrews-Hanna, J. R., & Schacter, D. L. (2008). The brain's default network. Annals of the New York Academy of Sciences, 1124(1), 1-38.

Bullmore, E., & Sporns, O. (2012). The economy of brain network organization. Nature Reviews Neuroscience, 13(5), 336-349.

Calhoun, V. D., & Adali, T. (2012). Multisubject independent component analysis of fMRI: a decade of intrinsic networks, default mode, and neurodiagnostic discovery. IEEE reviews in biomedical engineering, 5, 60-73.

Cecchin, D., Palombit, A., Castellaro, M., Silvestri, E., Bui, F., Barthel, H., Sabri, O., Corbetta, M., Bertoldo, A. (2017 Jul 27). Brain PET and functional MRI: why simultaneously using hybrid PET/MR systems? The Quarterly Journal of Nuclear Medicine and Molecular Imaging.

Cha, J., Hwang, J. M., Jo, H. J., Seo, S. W., Na, D. L., & Lee, J. M. (2015). Assessment of functional characteristics of amnestic mild cognitive impairment and Alzheimer’s disease using various methods of resting-state FMRI analysis. BioMed research international, 2015.

Chételat, G., Desgranges, B., de la Sayette, V., Viader, F., Eustache, F., Baron, J. C. (2003 Apr 22). Mild cognitive impairment: Can FDG-PET predict who is to rapidly convert to Alzheimer's disease? Neurology, 60(8), 1374-7.

Chételat G, Desgranges B, Landeau B, Mézenge F, Poline JB, de la Sayette V, Viader F, Eustache F, Baron JC. (2008 Jan). Direct voxel-based comparison between grey matter hypometabolism and atrophy in Alzheimer's disease. Brain,131,60-71.

Chételat, G., Villain, N., Desgranges, B., Eustache, F., Baron, J. C. (2009 Dec). Posterior cingulate hypometabolism in early Alzheimer's disease: what is the contribution of local atrophy versus disconnection? Brain,132(Pt 12),e133.

Cohen J. Statistical Power Analysis for the Behavioral Sciences. (1988). New York, NY: Routledge Academic

Cox, R. W. (1996). AFNI: software for analysis and visualization of functional magnetic resonance neuroimages. Computers and Biomedical research, 29(3), 162-173.

Cox, R. W. (2012). AFNI: what a long strange trip it's been. Neuroimage, 62(2), 743-747.

Damoiseaux, J. S., Prater, K. E., Miller, B. L., & Greicius, M. D. (2012). Functional connectivity tracks clinical deterioration in Alzheimer's disease. *Neurobiology of aging*, *33*(4), 828-e19.

Damoiseaux, J. S. Effects of aging on functional and structural brain connectivity. (2017 Feb 1). Neuroimage. pii: S1053-8119(17)30101-5.

Delso, G., Fürst, S., Jakoby, B., Ladebeck, R., Ganter, C., Nekolla, S. G., Schwaiger, M., & Ziegler, S. I. (2011). Performance measurements of the Siemens mMR integrated whole-body PET/MR scanner. Journal of nuclear medicine, 52(12), 1914-1922.

Dennis, E. L., & Thompson, P. M. (2014). Functional brain connectivity using fMRI in aging and Alzheimer's disease. Neuropsychology review, 24(1), 49.

Diaz-Ponce, A., Baláčková, N., Grönqvist, R., Rohra, H., Rockford-Brennan, H., Orheim, A., Doxford, H., Houston, A., Orheim, B., Ahola, M., Croy, A., Bentley, P., Henry, S., Ilieva, I.V., Ivanova, L., Mimica, N., Kušan Jukić, M., Diakou, A., Seleari, M., Holmerová, I., Mátlová, M., Vølund, B., Poulsen, S., Pajala, K., Decharry, P., Schönhof, B., Freter, H-J., Jansen, S., Poptsi, E., Lecca Marcati, E., Xatzidimitriou, G., Tsolaki, M., Kanaki, M., Giannouli, V., Maiori, X., Crean, M., Presti, M., Possenti, M., Blakey, M., Konevnina, A., Kuznecovs, V., Rasente, D., Macijauskiene, J., Adomaitiene, V., Mancini, D., Diederich, L., Scerri C., Pesce, A., Bordero, A., Palermiti, F., Nicaise, S., Louchart De La Chapelle, S., Van Klaveren, V., Brekke, L.A., Hov Eggen, S., Wojciechowska, M., Zincke dos Reis, M.R., Taudose, C. Moglan, M. Grniaková, D., Adamovicova, S., Zlobec, S., Selmes, M., Westerlund, K., Jarnryd, S., Wolfensberger, M., van der Poel, J.H., Kocaman, F. & Bentley, P. (2016). Dementia in Europe Yearbook 2016-Decision making and legal capacity in dementia.

Drevets, W. C., Bogers, W., Raichle, M. E. (2002 Dec). Functional anatomical correlates of antidepressant drug treatment assessed using PET measures of regional glucose metabolism. Eur Neuropsychopharmacol, 12(6), 527-44.

Drzezga, A., Barthel, H., Minoshima, S., & Sabri, O. (2014). Potential clinical applications of PET/MR imaging in neurodegenerative diseases. Journal of Nuclear Medicine, 55(Supplement 2), 47S-55S.

Dubois, B., Feldman, H. H., Jacova, C., Hampel, H., Molinuevo, J. L., Blennow, K., DeKosky S. T., & Cappa, S. (2014). Advancing research diagnostic criteria for Alzheimer's disease: the IWG-2 criteria. The Lancet Neurology, 13(6), 614-629.

Elseoud, A. A., Littow, H., Remes, J., Starck, T., Nikkinen, J., Nissilä, J., Timonen, M., Tervonen, O., & Kiviniemi, V. (2011). Group-ICA model order highlights patterns of functional brain connectivity. Frontiers in systems neuroscience, 5.

Fazekas, F., Chawluk, J. B., Alavi, A., Hurtig, H. I., Zimmerman, R.A. (1987 Aug). MR signal

abnormalities at 1.5 T in Alzheimer's dementia and normal aging. American Journal of Roentgenology, 149(2), 351-6.

Folstein, M. F., Folstein, S. E., McHugh, P. R. (1975). ‘‘Mini-mental state’’. A practical method for grading the cognitive state of patients for the clinician. Journal of Psychiatric Research, 12, 189–198.

Fox, P. T., Raichle, M. E., Mintun, M. A., & Dence, C. (1986). Nonoxidative glucose consumption during focal physiologic neural activity. Cell Biol, 102, 2076.

Goldberg, S., Smith, G. S., Barnes, A., Ma, Y., Kramer, E., Robeson, K., Kirshner, M., Pollock, B. G., Eidelberg, D. (2004 Feb). Serotonin modulation of cerebral glucose metabolism in normal aging. Neurobiology Aging, 25(2), 167-74.

Goldstone A, Mayhew SD, Przezdzik I, Wilson RS, Hale JR, Bagshaw AP. Gender Specific Re-organization of Resting-State Networks in Older Age. Front Aging Neurosci. 2016 Nov 25;8:285.

Grabner, G., Janke, A., Budge, M., Smith, D., Pruessner, J., & Collins, D. (2006). Symmetric atlasing and model based segmentation: an application to the hippocampus in older adults. Medical Image Computing and Computer-Assisted Intervention–MICCAI 2006, 58-66.

Greicius, M. D., Srivastava, G., Reiss, A. L., & Menon, V. (2004). Default-mode network activity distinguishes Alzheimer's disease from healthy aging: evidence from functional MRI. Proceedings of the National Academy of Sciences of the United States of America, 101(13), 4637-4642.

Guo, Z., Liu, X., Jia, X., Hou, H., Cao, Y., Wei, F., Li J., Chen, X., Zhang, Y., Shen, Y., Wei, L., Xu, L., & Chen, W. (2015). Regional coherence changes in alzheimer’s disease patients with depressive symptoms: a resting-state functional MRI study. Journal of Alzheimer's Disease, 48(3), 603-611.

Guo, Z., Liu, X., Li, J., Wei, F., Hou, H., Chen, X., Li, X., & Chen, W. (2017). Fractional amplitude of low-frequency fluctuations is disrupted in Alzheimer’s disease with depression. Clinical Neurophysiology, 128(7), 1344-1349.

Gusnard, D. A., & Raichle, M. E. (2001). Searching for a baseline: functional imaging and the resting human brain. Nature Reviews Neuroscience, 2(10), 685-694.

Hafkemeijer, A., van der Grond, J., & Rombouts, S. A. (2012). Imaging the default mode network in aging and dementia. Biochimica et Biophysica Acta (BBA)-Molecular Basis of Disease, 1822(3), 431-441.

Harris, J. J., Jolivet, R., & Attwell, D. (2012). Synaptic energy use and supply. Neuron, 75(5), 762-777.

Hyder, F., Herman, P., Bailey, C. J., Møller, A., Globinsky, R., Fulbright, R. K., Rothman, D. L., & Gjedde, A. (2016). Uniform distributions of glucose oxidation and oxygen extraction in gray matter of normal human brain: No evidence of regional differences of aerobic glycolysis. Journal of Cerebral Blood Flow & Metabolism, 36(5), 903-916.

Huang S, Zhou F, Jiang J, Huang M, Zeng X, Ding S, Gong H. (2017 Jun 6). Regional impairment of intrinsic functional connectivity strength in patients with chronic primary insomnia. Neuropsychiatr Dis Treat, 13, 1449-1462.

Ito, K., Fukuyama, H., Senda, M., Ishii, K., Maeda, K., Yamamoto, Y., Ouchi, Y., Ishii, K., Okumura, A., Fujiwara, K., Kato, T., Arahata, Y., Washimi, Y., Mitsuyama, Y., Meguro, K., Ikeda, M. (2015). Prediction of outcomes in mild cognitive impairment by using 18F-FDG-PET: a multicenter study. *Journal of Alzheimer's Disease*, *45*(2), 543-552.

Jenkinson, M., Beckmann, C. F., Behrens, T. E., Woolrich, M. W., & Smith, S. M. (2012). Fsl. Neuroimage, 62(2), 782-90.

Jenkinson, M., Pechaud, M., & Smith, S. (2005). BET2: MR-based estimation of brain, skull and scalp surfaces. In Eleventh Annual Meeting of the Organization for Human Brain Mapping.

Jones, D.T., Machulda, M.M., Vemuri, P., McDade, E.M., Zeng, G., Senjem, M.L., Gunter, J.L., Przybelski, S.A., Avula, R.T., Knopman, D.S., Boeve, B.F., Petersen, R.C., and Jack Jr., C. R. (2011). Age-related changes in the default mode network are more advanced in Alzheimer disease. Neurology, 77(16), 1524-31.

Kapogiannis, D., & Mattson, M. P. (2011). Disrupted energy metabolism and neuronal circuit dysfunction in cognitive impairment and Alzheimer's disease. The Lancet Neurology, 10(2), 187-198.

Kazemifar, S., Manning, K.Y., Rajakumar, N., Gómez, F. A., Soddu, A. , Borrie, M. J., Menon, R. S., Bartha, R., & Alzheimer’s Disease Neuroimaging Initiative. (2017). Spontaneous low frequency BOLD signal variations from resting-state fMRI are decreased in Alzheimer disease. PLoS One, 12(6), e0178529.

Kendall, M. G., & Gibbons, J. D. (1990). Rank Correlation Methods: Griffin.

Klaassens, B. L., van Gerven, J. M. A., van der Grond, J., de Vos, F., Moller, C., & Rombouts, S. (2017). Diminished Posterior Precuneus Connectivity with the Default Mode Network Differentiates Normal Aging from Alzheimer's Disease. Frontiers in aging neuroscience, 9.

Liu, Y., Wang, K., Yu, C., He, Y., Zhou, Y., Liang, M., Wang, L., Jiang, T. (2008). Regional homogeneity, functional connectivity and imaging markers of Alzheimer's disease: a review of resting-state fMRI studies. Neuropsychologia, 46(6), 1648-56.

Marchitelli, R., Collignon, O., & Jovicich, J. (2017). Test-Retest Reproducibility of the Intrinsic Default Mode Network: Influence of Functional Magnetic Resonance Imaging Slice-Order Acquisition and Head-Motion Correction Methods. Brain Connectivity, 7(2), 69-83.

McCabe, C., Mishor, Z. (2011 Aug). Antidepressant medications reduce subcortical-cortical resting-state functional connectivity in healthy volunteers. Neuroimage. 15, 57(4), 1317-23.

McGrath, R. E., Meyer, G. J. When effect sizes disagree: the case of r and d. (2006 Dec). Psychol Methods, 11(4), 386-401.

McKhann, G. M., Knopman, D. S., Chertkow, H., Hyman, B. T., Jack, C. R. Jr, Kawas, C. H., Klunk, W. E., Koroshetz, W. J., Manly, J. J., Mayeux, R., Mohs, R. C., Morris, J. C., Rossor, M. N., Scheltens, P., Carrillo, M. C., Thies, B., Weintraub, S., Phelps, C. H. (2011 May). The diagnosis of dementia due to Alzheimer's disease: recommendations from the National Institute on Aging-Alzheimer's Association workgroups on diagnostic guidelines for Alzheimer's disease. Alzheimer’s & Dementia, 7(3), 263-269.

Mergenthaler, P., Lindauer, U., Dienel, G. A., & Meisel, A. (2013). Sugar for the brain: the role of glucose in physiological and pathological brain function. Trends in neurosciences, 36(10), 587-597.

Minoshima, S., Giordani, B., Berent, S., Frey, K. A., Foster, N. L., & Kuhl, D. E. (1997). Metabolic reduction in the posterior cingulate cortex in very early Alzheimer's disease. Ann Neurol, 42(1), 85-94.

Montembeault, M., Rouleau, I., Provost, J.-S., & Brambati, S. M. (2016). Altered Gray Matter Structural Covariance Networks in Early Stages of Alzheimer’s Disease. *Cerebral Cortex (New York, NY)*, *26*(6), 2650–2662.

Mosconi, L. (2005). Brain glucose metabolism in the early and specific diagnosis of Alzheimer's disease. FDG-PET studies in MCI and AD. European journal of nuclear medicine and molecular imaging, 32(4), 486-510.

Nagata, K., Kondoh, Y., Atchison, R., Sato, M., Satoh, Y., Watahiki, Y., Hirata, Y., Yokoyama, E. (2000). Vascular and metabolic reserve in Alzheimer's disease. Neurobiology of aging, 21(2), 301-307.

Nagata, K., Sato, M., Satoh, Y., Watahiki, Y., Kondoh, Y., Sugawara, M., Box, G., Wright, D., Leung, S., Yuya, H., Shimosegawa, E. (2002 Nov). Hemodynamic aspects of Alzheimer's disease. Ann N Y Acad Sci, 977:391-402.

Nicolakakis, N., & Hamel, E. (2011). Neurovascular function in Alzheimer's disease patients and experimental models. Journal of Cerebral Blood Flow & Metabolism, 31(6), 1354-1370.

Nisbet, R. M., Polanco, J. C., Ittner, L. M., & Gotz, J. (2015). Tau aggregation and its interplay with amyloid-beta. Acta neuropathologica, 129(2), 207-220.

Nordberg, A. (2010). Amyloid imaging in early detection of Alzheimer's disease. Neurodegenerative Diseases, 7(1-3), 136-138.

Petersen, R. C., Roberts, R. O., Knopman, D. S., Boeve, B. F., Geda, Y. E., Ivnik, R. J., Smith, G. E., Jack, C. R. Jr. (2009 Dec). Mild cognitive impairment: ten years later. Archives of neurology, 66(12), 1447-55.

Poldrack, R. A., Baker, C. I., Durnez, J., Gorgolewski, K. J., Matthews, P. M., Munafò, M. R., Nichols, T. E., Poline, J. B., Vul, E., Yarkoni, T. (2017 Feb). Scanning the horizon: towards transparent and reproducible neuroimaging research. Nature Reviews Neuroscience,18(2), 115-126.

Power, J. D., Barnes, K. A., Snyder, A. Z., Schlaggar, B. L., & Petersen, S. E. (2012). Spurious but systematic correlations in functional connectivity MRI networks arise from subject motion. Neuroimage, 59(3), 2142-54.

Quarantelli, M., Berkouk, K., Prinster, A., Landeau, B., Svarer, C., Balkay, L., Alfano, B., Brunetti, A., Baron, J.C., Salvatore, M., 2004. Integrated software for the analysis of brain PET/SPECT studies with partial-volume-effect correction. J. Nucl. Med. 45, 192–201.

Rahim, M., Thirion, B., Abraham, A., Eickenberg, M., Dohmatob, E., Comtat, C., & Varoquaux, G. (2015). Integrating Multimodal Priors in Predictive Models for the Functional Characterization of Alzheimer’s Disease. Medical Image Computing and Computer Assisted Intervention.

Riedl, V., Bienkowska, K., Strobel, C., Tahmasian, M., Grimmer, T., Forster, S., Friston, J. K., Sorg, C., and Drzezga, A. (2014). Local activity determines functional connectivity in the resting human brain: a simultaneous FDG-PET/fMRI study. Journal of neuroscience, 34(18), 6260-6266.

Sambataro, F., Wolf, N., Pennuto, M., Vasic, N., & Wolf, R. (2014). Revisiting default mode network function in major depression: Evidence for disrupted subsystem connectivity. Psychological Medicine,44(10), 2041-2051.

Sarazin, M., Chauvire, V., Gerardin, E., Colliot, O., Kinkingnehun, S., de Souza, L. C., Hugonot-Diener, L., Garnero, L., Lehéricy, S., Chupin, M., Dubois, B. (2010). The amnestic syndrome of hippocampal type in Alzheimer's disease: an MRI study. Journal of Alzheimer's disease, 22(1), 285-294.

Shidahara, M., Tsoumpas, C., Hammers, A., Boussion, N., Visvikis, D., Suhara, T., Kanno, I., Turkheimer, F. E.. (2009). Functional and structural synergy for resolution recovery and partial volume

correction in brain PET. NeuroImage. 44, 2, 340–8.

Simpson, I. A., Carruthers, A., & Vannucci, S. J. (2007). Supply and demand in cerebral energy metabolism: the role of nutrient transporters. Journal of Cerebral Blood Flow & Metabolism, 27(11), 1766-1791.

Smith, S. M. (2002). Fast robust automated brain extraction. Human Brain Mapping, 17(3), 143-55.

Smith, S. M., Jenkinson, M., Woolrich, M. W., Beckmann, C. F., Behrens, T. E., Johansen-Berg, H., Bannister, P. R., De Luca, M., Drobnjak, I., Flitney, D. E., Niazy, R. K., Saunders, J., Vickers, J., Zhang, Y., De Stefano, N., Brady, J. M., Matthews, P. M. (2004). Advances in functional and structural MR image analysis and implementation as FSL. Neuroimage, 23 Suppl 1, S208-19.

Smitha, K. A., Akhil Raja, K., Arun, K. M., Rajesh, P. G., Thomas, B., Kapilamoorthy, T. R., & Kesavadas, C. (2017). Resting state fMRI: A review on methods in resting state connectivity analysis and resting state networks. The Neuroradiology Journal, 1971400917697342

Supekar, K., Menon, V., Rubin, D., Musen, M., & Greicius, M. D. (2008). Network analysis of intrinsic functional brain connectivity in Alzheimer's disease. PLoS computational biology, 4(6), e1000100.

Tahmasian, M., Eggers, C., Riedl, V., Sorg, C., & Drzezga, A. (2015). Editorial: Utilization of Hybrid PET/MR in Neuroimaging. Basic and clinical neuroscience, 6(3), 143.

Vaishnavi, S. N., Vlassenko, A. G., Rundle, M. M., Snyder, A. Z., Mintun, M. A., & Raichle, M. E. (2010). Regional aerobic glycolysis in the human brain. Proceedings of the National Academy of Sciences, 107(41), 17757-17762.

Vemuri, P., Jones, D. T., & Jack, C. R. (2012). Resting state functional MRI in Alzheimer's Disease. Alzheimer's Research & Therapy, 4(1), 2.

Varrone A1, Asenbaum S, Vander Borght T, Booij J, Nobili F, Någren K, Darcourt J, Kapucu OL, Tatsch K, Bartenstein P, Van Laere K; European Association of Nuclear Medicine Neuroimaging Committee. EANM procedure guidelines for PET brain imaging using [18F]FDG, version 2. Eur J Nucl Med Mol Imaging. 2009 Dec;36(12):2103-10.

Xie, C., Bai, F., Yuan, B., Yu, H., Shi, Y., Yuan, Y., Wu, D., Zhang, Z., Zhang, Z. (2015). Joint effects of gray matter atrophy and altered functional connectivity on cognitive deficits in amnestic mild cognitive impairment patients. Psychological Medicine, 45(9), 1799-1810.

Wehrl, H. F., Sauter, A. W., Divine, M. R., & Pichler, B. J. (2015). Combined PET/MR: a

technology becomes mature. Journal of Nuclear Medicine, 56(2), 165-168.

Yakushev, I., Landvogt, C., Buchholz, H. G., Fellgiebel, A., Hammers, A., Scheurich, A., Schmidtmann, I., Gerhard, A., Schreckenberger, M., Bartenstein, P., (2007). The choice of the reference area in 18F-FDG brain PET imaging of Alzheimer's disease. Psychiatry Research.

Yakushev, I., Landvogt, C., Buchholz, H. G., Fellgiebel, A., Hammers, A., Scheurich, A., Schmidtmann, I., Gerhard, A., Schreckenberger, M., Bartenstein, P. (2008 Nov 30). Choice of reference area in studies of Alzheimer's disease using positron emission tomography with fluorodeoxyglucose-F18. Psychiatry Research, 164(2), 143-53.

Yap, K. H., Ung, W. C., Ebenezer, E. G. M., Nordin, N., Chin, P. S., Sugathan, S., Chan, S. C., Yip, H. L., Kiguchi, M., Tang, T. B. (2017 Sep 1). Visualizing Hyperactivation in Neurodegeneration Based on Prefrontal Oxygenation: A Comparative Study of Mild Alzheimer's Disease, Mild Cognitive Impairment, and Healthy Controls. Frontiers in Aging Neuroscience, 9:287.

Yeo, B. T., Krienen, F. M., Sepulcre, J., Sabuncu, M. R., Lashkari, D., Hollinshead, M., Roffman., J. L., Smoller, J. W., Zöllei, L., Polimeni, J. R., Fischl, B., Liu, H., Buckner, R. L. (2011). The organization of the human cerebral cortex estimated by intrinsic functional connectivity. *Journal of neurophysiology*, *106*(3), 1125-1165.

Zang, Y., Jiang, T., Lu, Y., He, Y., & Tian, L. (2004). Regional homogeneity approach to fMRI data analysis. Neuroimage, 22(1), 394-400.

Zhang, H. Y., Wang, S. J., Liu, B., Ma, Z. L., Yang, M., Zhang, Z. J., & Teng, G. J. (2010). Resting brain connectivity: changes during the progress of Alzheimer disease. Radiology, 256(2), 598-606.

Zhou, M., Hu, X., Lu, L., Zhang, L., Chen, L., Gong, Q., & Huang, X. (2017). Intrinsic cerebral activity at resting state in adults with major depressive disorder: A meta-analysis. Progress in Neuro-Psychopharmacology and Biological Psychiatry, 75, 157-164.

Zou, Q. H., Zhu, C. Z., Yang, Y., Zuo, X. N., Long, X. Y., Cao, Q. J., Wang, Y. F., Zang, Y. F. (2008). An improved approach to detection of amplitude of low-frequency fluctuation (ALFF) for resting-state fMRI: fractional ALFF. *Journal of neuroscience methods*, *172*(1), 137-141.

Zuo, X. N., Di Martino, A., Kelly, C., Shehzad, Z. E., Gee, D. G., Klein, D. F., Castellanos, F. X., Biswal, B., Milham, M. P. (2010). The oscillating brain: complex and reliable. Neuroimage, 49(2), 1432-45.

Group	No. of subjects	Age	Gender (F/M)	MMSE (/30)	CDR	AChEI/ Antidepressants /both
aMCI	6	68.5 (4.7, 65-71)	1/5	26.0 (0.7, 26-29)	0.5	1/1/1
AD	17	72.0 (6.0, 54-84)	7/10	2.01 (3.8, 16-26)	1.0 (1.0, 1-2)	5/3/3
All patients	23	71.0 (5.5, 54-84) ***	8/15 **	23.5 (6.0, 16-29) ***	1.0 (1.0, 0.5-2)	6/4/4
HC	23	64 (13, 43-76)	16/7	29 (2.0, 28-30)	0	0/0

Table 1. Clinical and demographic features. The table reports the medians (numbers in parentheses are IQR and ranges) for age (in years), MMSE and CDR scores, within each specific group of aMCI patients and AD patients as well as all patients and neurologically healthy controls, respectively. For each group, the number of subjects , their gender (F/M) and treatment are also reported. aMCI: amnestic mild cognitive impairment, AD: Alzheimer Disease, MMSE: Mini-Mental State Examination, CDR: Clinical Dementia Rating Score. AChEI: acetylcholinesterase inhibitors. Statistics were performed between all patients versus neurologically healthy controls(bottom rows). ** $p<0.01$ all patients vs controls; *** $p<0.001$.

Molecular & Functional Activity Measurement	COM Location (Talairach-Tournoux Atlas)	Clusters Size (Voxels)	COM coordinates (RAI order)
FDG-PET	R/L Precuneus	4581	-1.6 +54.2 +33.8
	R Superior Temporal gyrus	4317	-52.3 +48.8 +13.6
	L Superior Temporal gyrus	3952	+51.2 +49.9 +9.9
	L Middle Frontal gyrus	3108	+7.0 -42.0 +22.1
	L Thalamus & L Medial Dorsal Nucleus	993	+2.2 +20.9 +5.8
	R Middle Frontal gyrus	553	-35.3 -16.5 +48.9
	R Middle Frontal gyrus & R Superior Frontal gyrus	503	-27.1 -58.1 +14.1
fALFF	R/L Cingulate gyrus & R/L Precuneus	679	-0.8 +42.9 +41.9
	R/L Middle Frontal gyrus	423	-0.8 -45.6 +24.0
ReHo	R Supra-marginal gyrus & R Inferior Parietal Lobule	1082	-49.7 +54.3 +37.4
	R/L Precuneus	923	-1.4 +60.0 +36.0
	L Angular gyrus & L Inferior Parietal Lobule	911	+49.1 -59.8 +36.4
gICA-DR	R/L Precuneus	419	-1.9 +64.6 +42.4

Table 2. Brain regions significantly affected in aMCI/AD in the between-group statistical analysis. This table summarizes the regions exhibiting reduced glucose consumption and loss of intrinsic functional activity and connectivity. From left to right, columns indicate the variables of interest, the location of the centre-of-mass (COM) of the significant cluster, cluster size in number of voxels, and COM coordinates. The reported regions include those found within 2mm radius from the COM. Coordinates are defined based on the MNI template and follow the RAI order. FDG-PET showed the largest clusters, more numerous than found with rs-fMRI. The region of the precuneus is consistently involved across all variables and imaging modalities. R/L = right/left. COM = centre of mass. RAI = right/anterior/inferior. FDG-PET = fluorodeoxyglucose positron emission tomography. fALFF = fractional amplitude of low frequency fluctuations; ReHo = regional homogeneity. gICA-DR = group independent component analysis and dual regression.

Molecular/Functional Correlation	COM Location (Talairach-Tournoux Atlas)	Clusters Size (Voxels)	COM coordinates (RAI order)
FDG-PET/fALFF	R Caudate & R Caudate Body	632	-12.8 +1.3 12.5
	L Thalamus & L Ventral Anterior Nucleus	618	+12.0 +4.6 +11.7
	R/L mid-cingulate gyrus	557	-0.9 +7.8 +40.2
	L Middle Frontal gyrus & L Superior Frontal gyrus	494	+29.5 -42.9 +29.7
	R/L Middle Frontal gyrus	435	-0.8 -46.2 +28.9
	L Inferior Parietal Lobule & L Superior Frontal Lobule	397	+43.5 +61.1 +48.2
	R Middle Frontal gyrus	337	-35.4 -45.0 +23.8
FDG-PET/ReHo	L Inferior Parietal Lobule & L Supramarginal gyrus	1221	+49.6 +58.8 +39.3
	R Inferior Parietal Lobule & R Supramarginal gyrus	1078	-51.4 +55.5 +39.2
	R/L Posterior Cingulate gyrus	981	-0.4 +28.8 +38.4
FDG-PET/gICA-DR	R/L Posterior Cingulate gyrus & R/L Precuneus	3261	0.0 +53.7 +29.0
	R Middle Frontal gyrus	668	-26.8 -31.4 +40.5
	L Supramarginal gyrus & L Angular gyrus & L Superior Temporal gyrus	566	+46.9 +59.8 +30.4
	R Superior Temporal gyrus & R Middle Temporal gyrus	346	-45.5 +56.6 +22.5

Table 3. Summary for across-subject clusters of correlations. This table shows size and location of main clusters derived from significant positive partial correlations between FDG-PET and RS-fMRI measures. Only correlations > +0.2 forming clusters larger than 300 voxels are here considered. From left-to-right, columns show the RS-fMRI measure considered, the location of COM on the Talairach-Tournoux atlas, the cluster-size in terms of number of voxels and COM coordinates. Coordinates are defined on the MNI template and follow the RAI order. RS-fMRI measures did not perfectly agree in terms of their spatial distribution when correlated to metabolic glucose consumption. The largest cluster was observed in the Precuneus for gICA-DR. ReHo and gICA-DR were correlated to glucose distribution mostly in posterior regions and overlap more with the DMN. fALFF showed the smallest number of clusters, with the most of them located in frontal regions. R/L = right/left. COM = centre of mass. RAI = right/anterior/inferior. FDG-PET = Fludeoxyglucose positron emission tomography. fALFF = fractional amplitude of low frequency fluctuations; ReHo = regional homogeneity. gICA-DR = group independent component analysis and dual regression. DMN = default mode network.

Statistical FDG-PET/fMRI contrast	COM Location (Talairach-Tournoux Atlas)	Clusters Size (Voxels)	COM coordinates (RAI order)
fALFF > ReHo	L Middle Frontal gyrus	572	+29 -45 +28
	L Superior Medial Frontal gyrus	419	+0.4 -45.8 +29.3
	R Middle Frontal gyrus	388	-36 -46 +22.3
fALFF > gICA-DR	L Middle Frontal gyrus	599	+29.7 -45.4 +26.8
	L Superior Medial gyrus	513	-0.7 -43.9 +29
	R Middle Frontal gyrus	411	-35.9 -46.4 +22.1
ReHo > fALFF	L Angular gyrus	807	+51.2 +58.1 +37.4
	R Angular gyrus	676	-51.6 +60 +34
	R Inferior Frontal gyrus (p. Orbitalis)	362	-21.8 -15.1 -25.1
ReHo > gICA-DR	L Angular gyrus	915	+50.9 +57.5 +38.4
	R Angular gyrus	845	-53 +56 +37.1
	R Inferior Frontal gyrus	332	-19.6 -14.7 -24.8
gICA-DR > ReHo	N.A.	N.A.	No significant voxels found
gICA-DR > fALFF	R Posterior Cingulate cortex	582	-5.9 +46.5 +31.5

Table 4. Highest-ranked across-subject FDG-PET/fMRI correlations compared across rs-fMRI metrics. This table shows size and location of the highest-ranked clusters for across-subject FDG-PET/fMRI correlations according to the voxelwise Friedman test, corrected for multiple comparisons using post-hoc voxelwise paired t-tests. Only clusters larger than 300 voxels are here considered ($p<0.001$). From left-to-right, columns show the statistical contrast depending on rs-fMRI metrics, the location of COM on the Talairach-Tournoux atlas, the cluster-size in terms of number of voxels and COM coordinates. Coordinates are defined on the MNI template and follow the RAI order. Compared with other rs-fMRI metrics, fALFF showed statistically significant clusters in Frontal regions. ReHo showed statistically significant clusters in Inferior Parietal regions. gICA-DR showed statistically significant clusters in the PCC compared with fALFF only. R/L = right/left. COM = centre of mass. RAI = right/anterior/inferior. FDG-PET = Fludeoxyglucose positron emission tomography. fALFF = fractional amplitude of low frequency fluctuations; ReHo = regional homogeneity. gICA-DR = group independent component analysis and dual regression. PCC = Posterior Cingulate cortex.

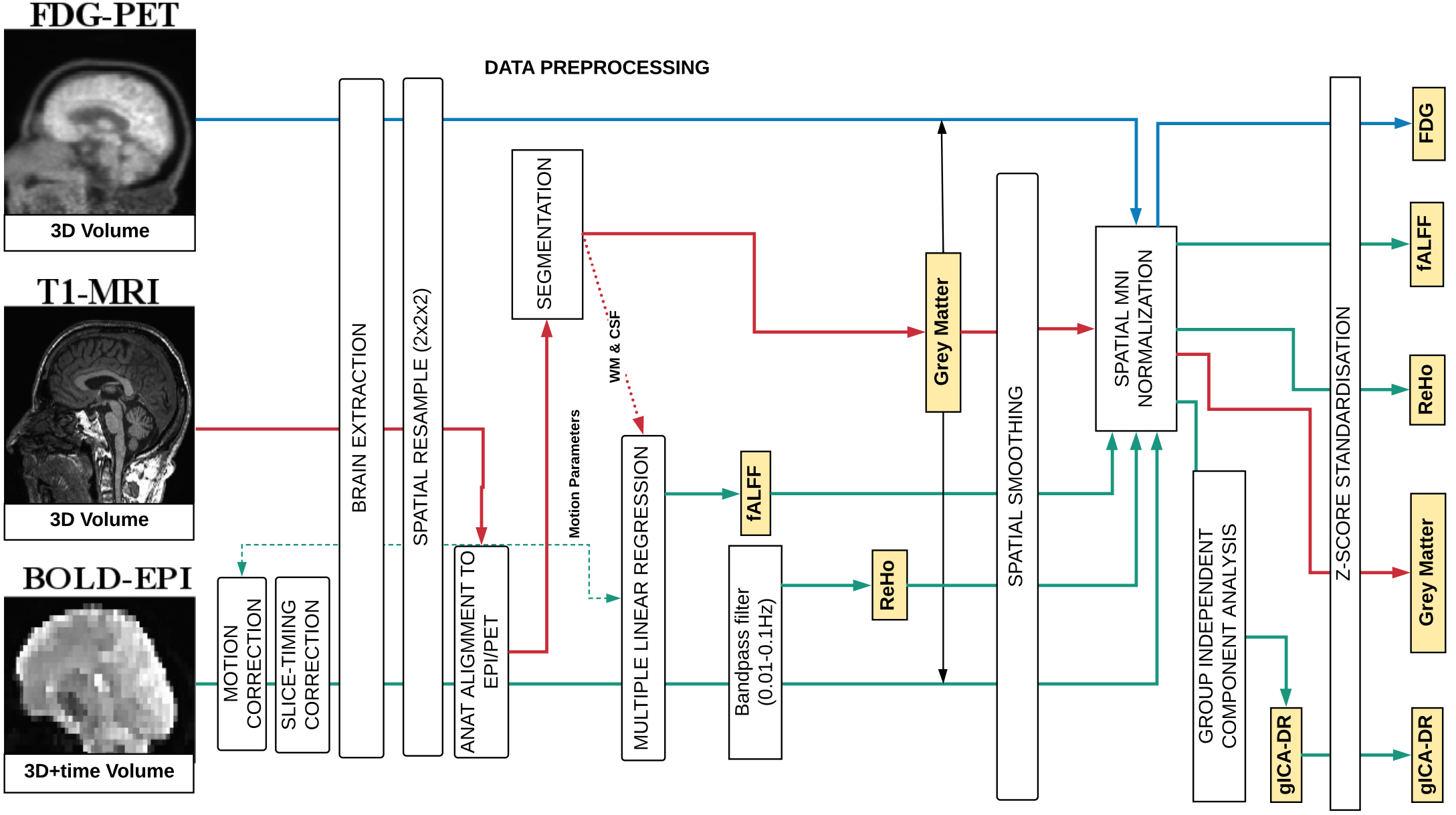

Figure 1: Preprocessing of RS-fMRI, FDG-PET and T1-MPRAGE data. This flowchart shows data preprocessing steps and order for FDG-PET (blue line), T1-MPRAGE (red line) and RS-fMRI BOLD data (green line) in the individual space. The dotted lines indicate parallel processes that do not undergo data preprocessing, i.e. motion and WM/ CSF timeseries. Metabolic and functional measures are highlighted in yellow-filled squares. See data preprocessing for more details.

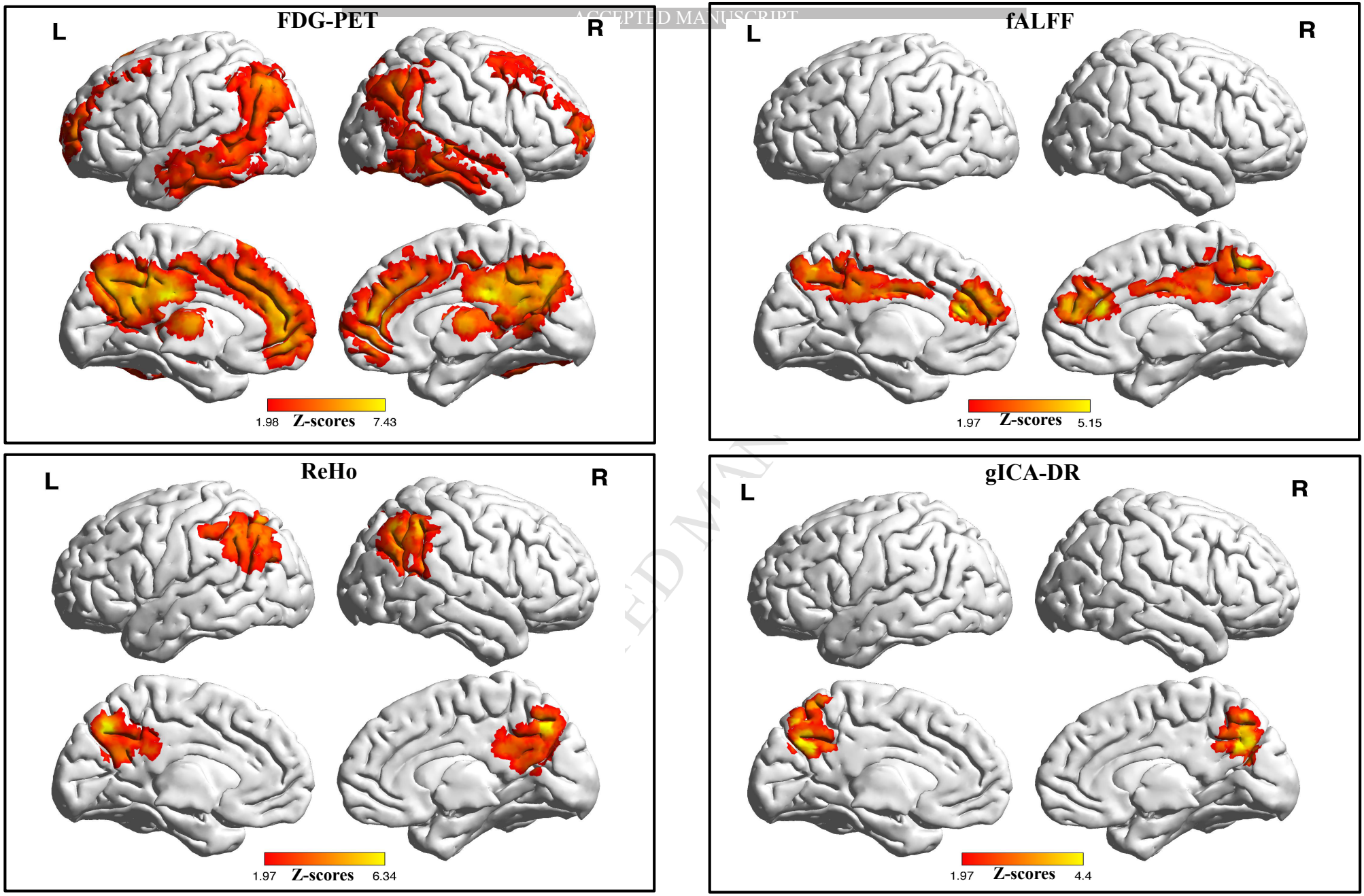

Figure 2: Impact of AD/aMCI pathology on brain metabolism and function. The figure shows MNI surface rendering with both lateral and sagittal views, overlaid with results from the between-group statistical analysis using the CTRL > AD contrast. These are separately presented for each imaging modality and metric evaluated, showing: **top-left:** AD-related glucose hypo-metabolic regions; **top right:** reduced fALFF; **bottom left:** reduced ReHo; **bottom right:** reduced functional DMN connectivity from gICA-DR. Glucose hypo-metabolism shows the most extensive spatial distribution whereas gICA-DR exhibits the smallest one. All measures overlap in the precuneus. The three fMRI parameters diverge with respect to frontal and temporo-parietal regions. These results are expressed as Z-scores ($p<0.05$) and are corrected for false-positive clusters using alphasym ($alpha<0.05$). Results from the opposite contrast (AD>CTRL) did not survive alphasym correction.

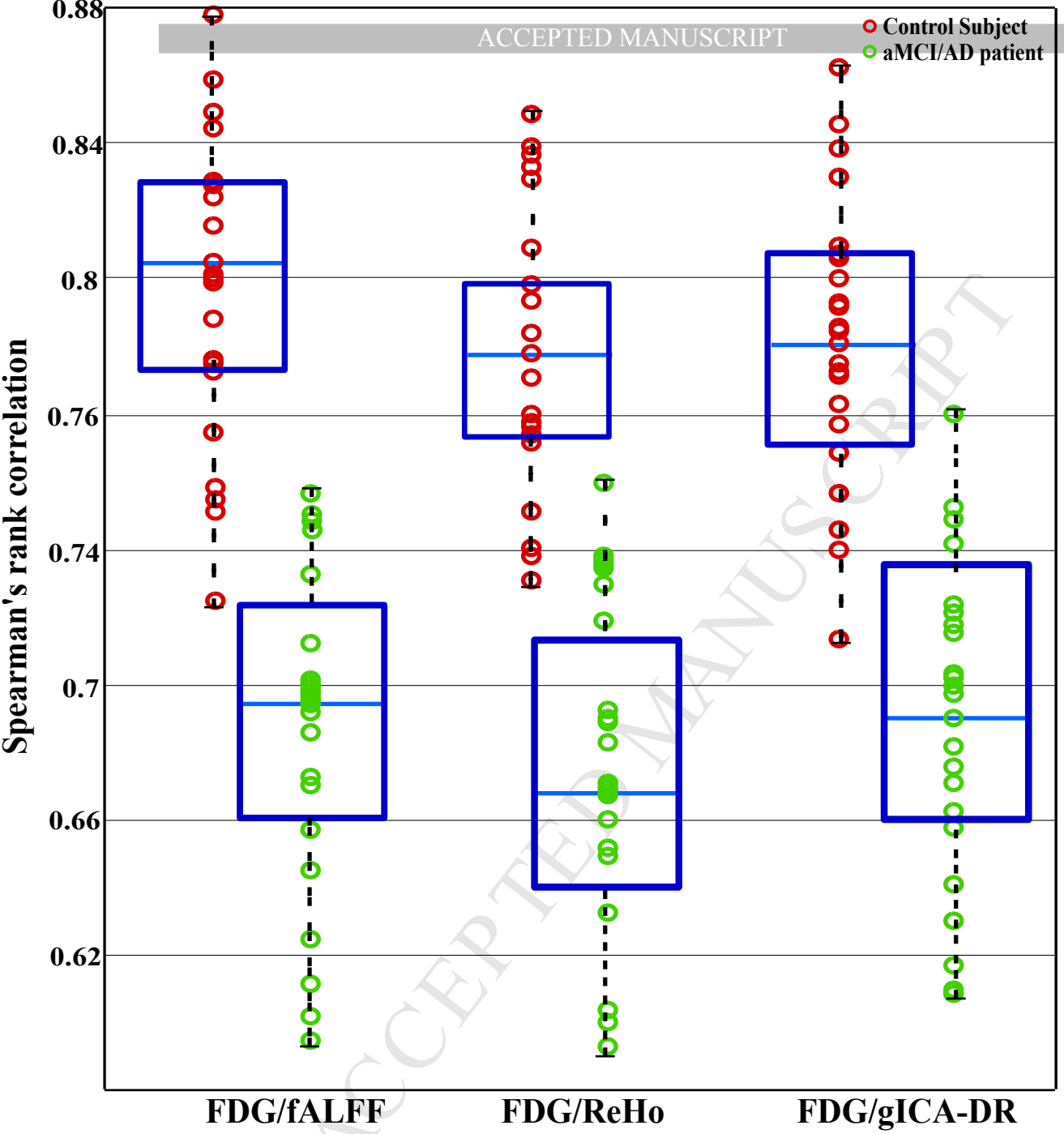

Figure 3: Resting-state FDG/fMRI correlations within grey matter voxels in individual subjects (N=46). Spearman's rank partial correlations between resting-state FDG-PET and BOLD-fMRI metrics are shown for each neurologically healthy old subject (green circles) and aMCI/AD patients (red circles). The strength of correlations is shown on the y-axis while correlations with FDG are shown on the x-axis, for each rs-fMRI metric such as fALFF, ReHo, gICA-DR (from-left-to-right). Correlations were overall significant and positive across all subjects, with no statistically significant difference across rs-fMRI metrics. Early aMCI/AD patients show statistically significant reduction in mean correlations compared to controls, for any rs-fMRI metric. Each dark-blue box is the IQR with median as the light-blue central mark. Black whiskers extend to the most extreme non-outlier datapoints.

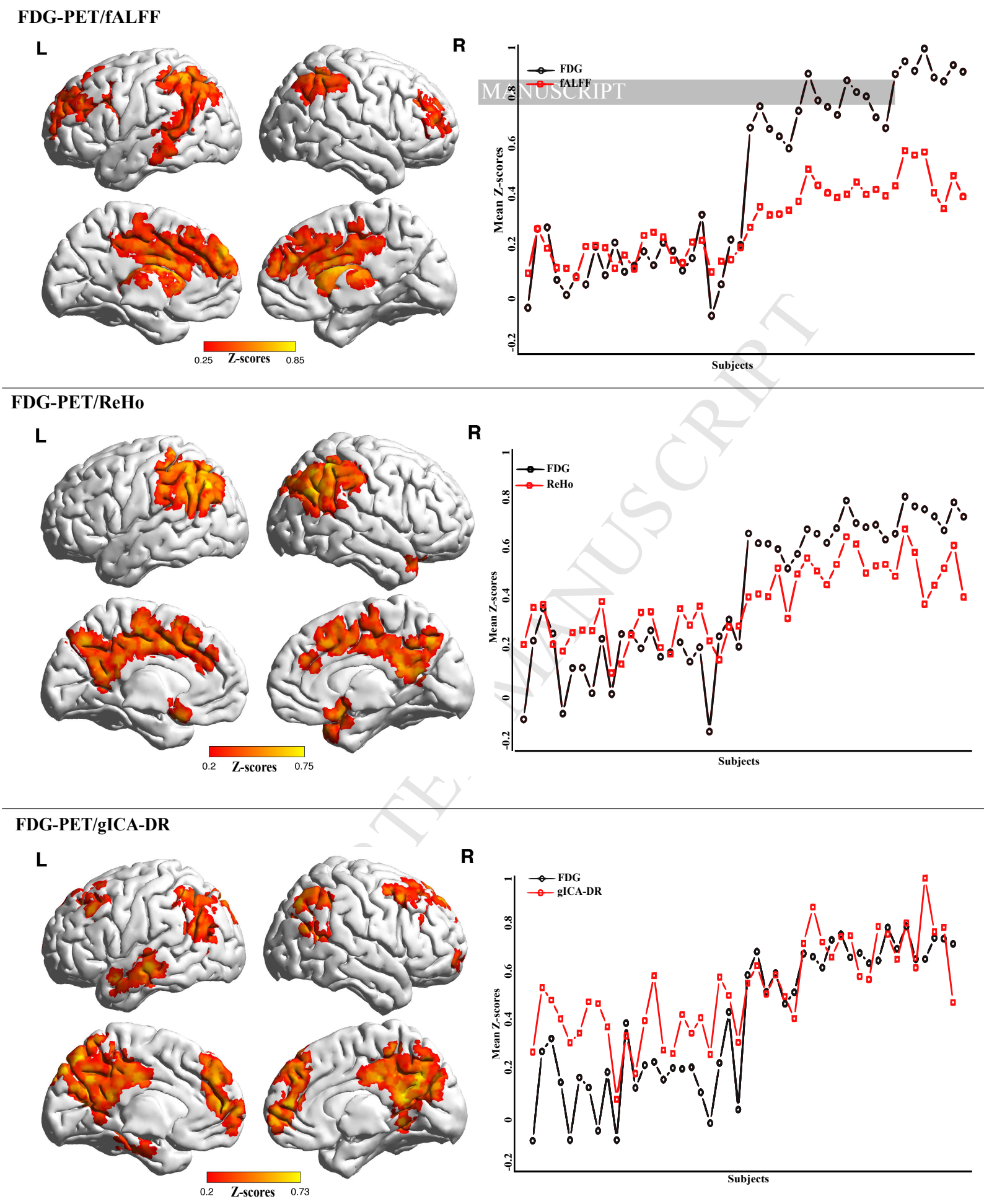

Figure 4: Across-subject correlations between FDG-PET and RS-fMRI metrics. The left part of the figure shows MNI surface rendering with both lateral and sagittal views, overlaid with the voxelwise correlations, corrected for GM density, across all individuals between FDG-PET and fALFF(**top panel**), ReHo (**middle**) and gICA-DR (**bottom**). These variables were positively correlated in regions typically affected by the disease process, particularly with respect to ReHo and gICA-DR. No correlations were found in the precuneus and posterior cingulate cortex for fALFF. Negativ correlations were not statistically significant and mostly located at the grey/white matter borders. For each correlation sub-type, the mean Z-scores averaged from highlighted regions are reported for each subject in the right panels.